Hayrettin YILDIZ

M.S. Thesis in Physics

February – 2010

SUPERPARAMAGNETIC RESONANCE STUDIES ON FERRITE NANOPARTICLES

by

Hayrettin YILDIZ

February 2010

SUPERPARAMAGNETIC RESONANCE STUDIES ON FERRITE NANOPARTICLES

by

Hayrettin YILDIZ

A thesis submitted to

the Graduate Institute of Sciences and Engineering

of

Fatih University

in partial fulfillment of the requirements for the degree of

Master of Science

in

Physics

February 2010
Istanbul, Turkey

APPROVAL PAGE

I certify that this thesis satisfies all the requirements as a thesis for the degree of Master of Science.

Prof. Dr. Mustafa KUMRU
Head of Department

This is to certify that I have read this thesis and that in my opinion it is fully adequate, in scope and quality, as a thesis for the degree of Master of Science.

Assoc. Prof. Dr. Yüksel KÖSEOĞLU
Supervisor

Examining Committee Members

Assoc. Prof. Dr. Yüksel KÖSEOĞLU ……..

Assoc. Prof. Dr. Sadık GÜNER…..……..

Assoc. Prof. Dr. Abdülhadi BAYKAL…..……

It is approved that this thesis has been written in compliance with the formatting rules laid down by the Graduate Institute of Sciences and Engineering.

Assoc. Prof. Dr. Nurullah ARSLAN
Director

February 2010

SUPERPARAMAGNETIC RESONANCE STUDIES ON FERRITE NANOPARTICLES

Hayrettin YILDIZ

M.S. Thesis – Physics
February 2010

Supervisor: Assoc. Prof. Dr. Yüksel KÖSEOĞLU

ABSTRACT

Magnetic nanoparticles have attracted great interest due to their mesoscopic properties and their potential for applications. In this study, the theory of the Superparamagnetic Resonance (SPR) and its application on magnetic nanoparticles $ZnFe_2O_4$ and $Co_{0.3}Zn_{0.7}Fe_2O_4$ were studied. The temperature dependent magnetic properties of these particles were investigated. Then these particles are considered as single magnetic domains with random orientations of magnetic moments and thermal fluctuations of anisotropic axes. The individual line shape function is derived from the damped precession equation of Landau-Lifshitz. Magnetic properties of the samples were strongly temperature and size dependent. When the temperature is decreased, while the SPR line width is increasing the resonance field is decreasing. This means the anisotropy field is increasing by decreasing the temperature. At high temperature, the SPR line shape is governed by the core anisotropy and the thermal fluctuations. On decreasing T, as the shell spins increase their magnetic susceptibility, they produce an effective field on the core, leading to a decrease of resonance (Br) from its high T value. As the shell spins begin to order, the effective anisotropy increases following its surface value more closely. So, the results can be interpreted by a simple model, in which

each single domain nanoparticle is considered as a core-shell system, with uniaxial anisotropy on the core and surface anisotropy on the shell.

Keywords: Superparamagnetic resonance, superparamagnetism, spinel structure, magnetic nanoparticles, $ZnFe_2O_4$, $Co_{0.3}Zn_{0.7}Fe_2O_4$.

FERRİTE NANOPARÇACIKLARDA SÜPERPARAMANYETİK REZONANS ÇALIŞMALARI

Hayrettin YILDIZ

Yüksek Lisans Tezi – Fizik
Şubat 2010

Tez Yöneticisi: Doç. Dr. Yüksel KÖSEOĞLU

ÖZ

Manyetik nanoparçacıklar uygulama alanlarının genişligi ve mezoskopik özelliklerinden dolayı çok yaygın olarak çalışılmaktadır. Bu çalışmada,Süperparamanyetik Rezonans (SPR) teorisi ve onun manyetik nanoparçacıklar $ZnFe_2O_4$ ve $Co_{0.3}Zn_{0.7}Fe_2O_4$ üzerindeki uygulaması çalışılmıştır. Sıcaklığa bağlı manyetik özellikleri araştırılmıştır. Rastgele yönelmiş manyetik momentler ve anizotropi ekseninin ısısal dalgalanmalarından dolayı bu nanoparçacıkların tek alanlı (single domain) oldukları kabul edilmiştir. Tek çizgi fonksiyonu Landau-Lifshitz'in sönümlü presesyon denkleminden elde edilmiştir. Numunelerin manyetik özeliklerinin büyüklüklerine ve sıcaklığa şiddetli bağımlı olduğu gözlenmiştir. Sıcaklık düşerken SPR çizgi genişliği artarak rezonans alanı azalmıştır. Bunun anlamı düşen sıcaklıkla anizotropi alanının artmasıdır. Yüksek sıcaklıklarda SPR çizgi şekli çekirdek anizotropisi ve ısısal dalgalanmalardan etkilenmiştir.

Azalan sıcaklıkla birlikte kabuk spinleri numunelerin manyetik alınganlığını artıracakları için bunlar çekirdek üzerinde etkin bir manyetik alan oluştururlar ve buda rezonans alanının (Br) yüksek sıcaklıklardaki değerinden daha küçük değerlere sahip olmasına sebep olur.

Anahtar Kelimeler: Süperparamanyetik rezonans,süperparamanyetizma, spinel yapılar, manyetik nanoparçacıklar, $ZnFe_2O_4$, $Co_{0.3}Zn_{0.7}Fe_2O_4$.

ACKNOWLEDGEMENT

Firstly, I would like to gratitude to my supervisor Assoc. Prof. Dr. Yüksel KÖSEOĞLU for his motivation, help, stimulating and incentive suggestions during whole time of research and for writing this thesis.

I want to thank to Prof. Dr. Mustafa KUMRU for his stimulation and motivation in my thesis.

I want to thank Assoc. Prof. Dr. Abdülhadi BAYKAL for valuable advices.

My special thanks go to Dr. Resul YILGIN for his heartfelt helps in measurement and valuable advices, motivation and collaboration in my thesis.

I also want to thank to Fatma GÖZÜAK for the synthesis and supply of the nanoparticles.

Finally I want to thank to my wife Nejla for her support and patience meanwhile I prepare this thesis. I also want to thank to my daughters Fatma and Dilara.

TABLE OF CONTENTS

LIST OF FIGURES

LIST OF SYMBOLS AND ABBREVIATIONS

SPR	:	Superparamagnetic resonance
SPM	:	Superparamagnetic
ESR	:	Electron spin resonance
EPR	:	Electron paramagnetic resonance
MNPs	:	Manufacturing the magnetic nanoparticles
FMR	:	Ferromagnetic resonance
DPPH	:	Diphenylpicrylhydrazyl, antioxidant free radical
ZFC	:	Zero field cooled
μ	:	The electronic or atomic moment
μ_s	:	Spin magnetic moment
m_{av}	:	Average magnetic moment
μ_r	:	Relative magnetic permeability
mo	:	Magnetic permeability of free space
A	:	Area
M	:	Magnetization vector
Ms	:	Saturation magnetization
N	:	Number of atoms
B	:	Total magnetic field
B_0	:	Applied (external) field
Hd	:	Demagnetizing filed
χ	:	Magnetic susceptibility
Tc	:	Curie temperature (Critical temperature)
T_N	:	Neél temperature
T_B	:	Blocking temperature
K	:	Anisotropy constant
fo	:	Attempt frequency
η	:	Dynamic viscosity
H_K	:	Internal magnetic field due to anisotropy

E ani	:	The magnetocrystalline anisotropy energy
C	:	Curie constant
K_b	:	Boltzman constant
h	:	Planck's constant
G	:	Magnetic field unit, gauss
T	:	Magnetic field unit, tesla
H	:	Effective magnetic field
dP/dH	:	First derivative of absorption peak
L(x)	:	Langevin function
G(y)	:	Superparamagnetic averaging factor
M_r	:	Remenance
Hc	:	Coercivity
Eexc	:	Heisenberg exchange energy
ω	:	Angular frequency
n	:	Larmour precession frequency
τ_0	:	Attempt period
τ_N	:	Relaxation time
V'	:	Hydrodynamic volume of the particle
Hr	:	Resonance field
DH	:	Line width
^oC	:	Centigrade degree
A^o	:	Angstrom
a.u.	:	Arbitrary unit.
γ	:	Gyromagnetic ratio constant

CHAPTER 1

INTRODUCTION

In physics, the fundamental interactions are the ways that individual particles interact with each other. It turns out that for every single interaction that we've observed take place in the universe, they can be broken down to be described by only four types of interactions. First interaction is gravity, the second one is electromagnetism, the third one is weak interaction and the fourth one is strong interaction. Many physicists believe that all four of the fundamental interactions (or forces) are, in fact, the manifestations of a single underlying (or unified) force which has yet to be discovered. Just as electricity, magnetism, and the weak force were unified into the electroweak interaction. The current quantum mechanical interpretation of these forces is that the particles do not interact directly, but rather manifest virtual particles that mediate the actual interactions. All of the forces except for gravity have been consolidated into this "Standard Model" of interaction [1].

Nanotechnology, shortened to "nanotech", is the study of the control of matter on atomic and molecular scale. Nanomaterial research studies materials with morphological features on the nanoscale, and especially those have special properties stemming from their nanoscale dimensions. Last decades, magnetic nanoparticles have attracted great interest due to their mesoscopic properties and their potential for applications. We know that there are a lot of applications of nanotechnology in today's life as shown in figure 1.1.

In recent years, there has been a growing demand for novel functional and transparent materials for non-linear optical devices, solid-state laser amplifiers and as transparent magnets. In particular, transparent magnets show great promise for magneto-optical recording, displays and holograms, as well as for magneto-optical solid devices in light wave

guides or photonic circuits, such as isolators, modulators and switches [2-5]. By incorporating nanophase magnetic particles into a polymer, glass or ceramic matrix, functional nanohybrids with many interesting optical and magnetic properties have been successfully synthesized [2, 6-10]. In these nanohybrids, transparency is affected by the absorption coefficients of both the magnetic nanoparticles and the matrix, as well as the configuration of their interfaces. The matrix phase also acts to control the in-situ formation and coarsening of nanoparticles during processing, minimising the optical scattering observed with embedded coarse particles and therefore enhancing the transparency [2].

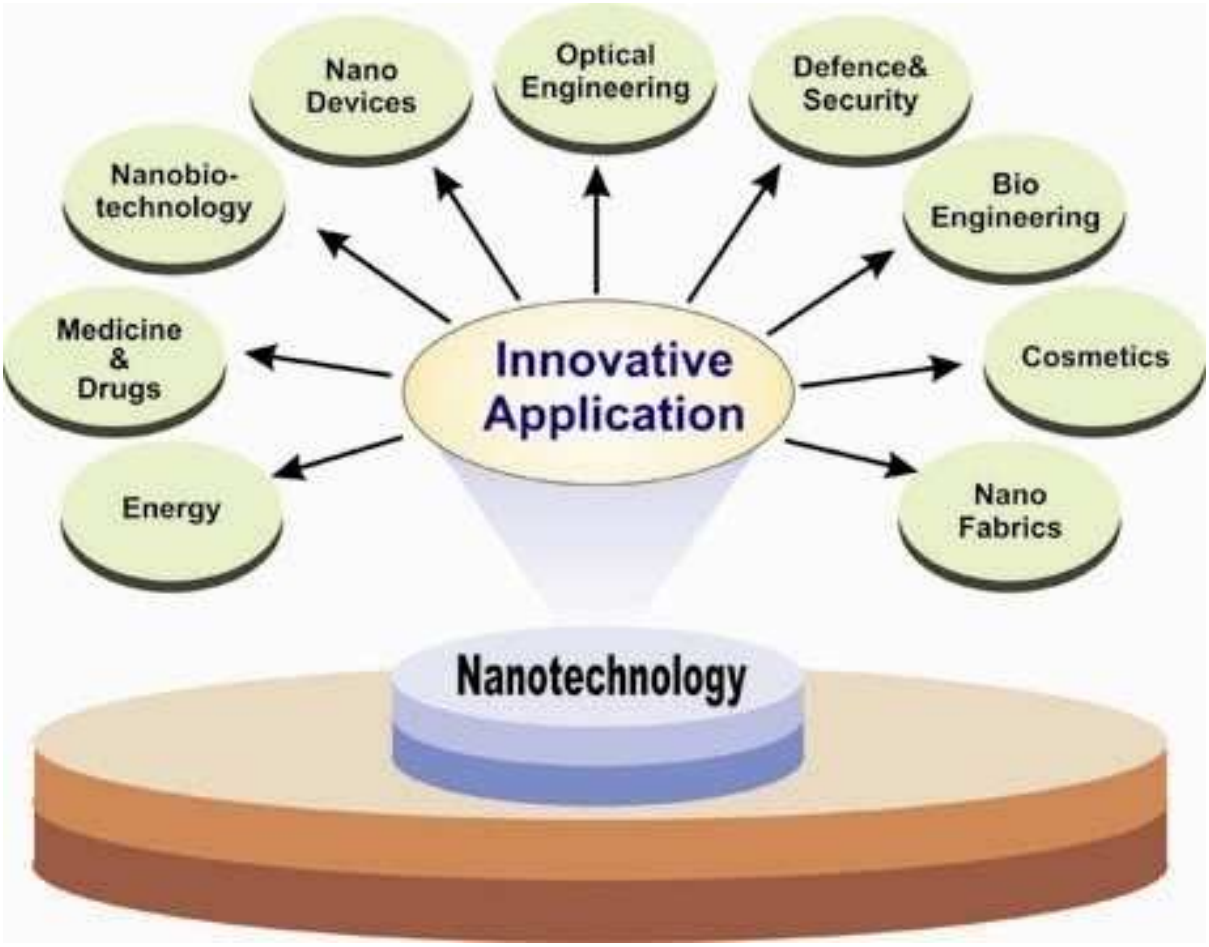

Figure 1.1 Diverse applications of nanotechnology in today's life [11].

Manufacturing the magnetic nanoparticles (MNPs) have started many years ago, and currently there are reliable synthesis routes. However, synthesis of MNPs with a few nanometers size, keeping the magnetic moment of the corresponding bulk material, is still a challenge because the high surface/volume ratio makes the surface disorder effect to be

dominant [12,13]. When the size of magnetic particles decreases into nanometer sized scale, the surface area increases greatly, resulting in novel phenomena. Superparamagnetism, magnetic quantum tunneling and spin-glass-like behavior are some examples in the field of nanomagnetism. These magnetic properties make magnetic nanoparticles to have many technological applications such as; recording tapes, permanent magnets, hard disc recording media, flexible recording media, read-write heads, active components of ferrofluids, color imaging, magnetic refrigeration, detoxification of biological fluids, magnetically controlled transport of anti-cancer drugs, magnetic resonance imaging (MRI) contrast enhancement and magnetic cell separation, etc [14-31]. Therefore, the development of different synthesis methods, by which materials having nanometer-sized grain size, retain the magnetic performance of the bulk materials, is still desirable [12]. Investigation of magnetic properties for these type of nanoparticles is still have increasing interest.

In this study, we consider superparamagnetic nanoparticles especially zinc ferrite $ZnFe_2O_4$ and cobalt doped zinc ferrite $Co_{0.3}Zn_{0.7}Fe_2O_4$ nanoparticles synthesized by microwave assisted combustion method and Polyethyle neglycol (PEG) assisted hydrothermal method. We used Electron Spin Resonance (ESR) technique to investigate magnetic properties of these nanoparticles. We measured the magnetic properties by varying the applied magnetic field and the temperature.

CHAPTER 2

CLASSIFICATION OF MAGNETIC MATERIALS

Magnetic materials may be classified by their response to externally applied magnetic field as diamagnetic, paramagnetic, ferromagnetic, antiferromagnetic, ferrimagnetic and superparamagnetic materials. And, they can be explained briefly as follows.

2.1 Magnetic Property

We know that all magnetic materials contain magnetic moments, which behave in a way similar to microscopic bar magnets. Let us consider concept of magnetic moment. In the atoms of many elements the electrons are arranged symmetrically so that the magnetic moments due to the spin and orbital motion cancel out, leaving the atom with zero magnetic moment. However the atoms of more than 1/3 rd of known elements lack this symmetry so that they (the atoms) do possess a magnetic moment. However in most of these materials the arrangement of the atoms is such that the magnetic moment of one is cancelled out by that of an oppositely directed near neighbours.

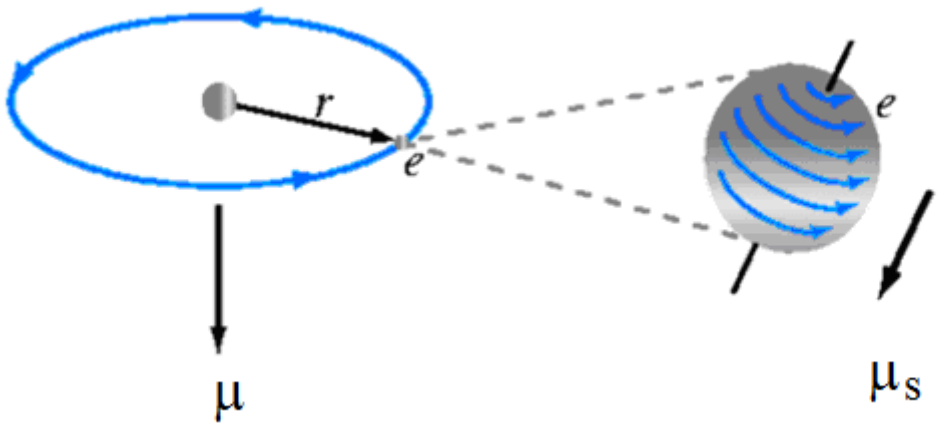

Figure 2.1 An electron has two types of rotation: orbital motion and spin motion [32].

The characteristics of the current loops are summarized in its magnetic moment. The magnetic moment can be considered to be a vector quantity with direction perpendicular to the current loop in the right-hand-rule direction. If we look at figure 2.1, the magnetic moment associated with this current loop is equal to current times area of the loop from Eq. 2.1.

$$\mu = IA \tag{2.1}$$

Where I is the current in the loop, $A = \pi r^2$ is the area enclosed by the orbit. We can use magnetic moments in a material to identify different forms of magnetism observed in nature.

2.1.1 Diamagnetism

Diamagnetism is a property of all materials and opposes to the externally applied magnetic fields, but is very weak. Why? Because the orbital motion of electrons creates tiny atomic current loops, which produce magnetic fields. When an external magnetic field is applied to a material, these current loops will tend to align in such a way as to oppose the applied field. This may be viewed as an atomic version of Lenz's law: induced magnetic fields tend to oppose the change which created them. Materials in which this effect is the only magnetic response are called diamagnetic. We consider electronic configurations of materials, diamagnetism is observed in materials with filled electronic sub-shells where the magnetic moments are paired and overall cancel each other. However, when exposed to a field, a negative magnetization is produced and thus the susceptibility (χ) is negative. If we plot M vs H and χ vs T, we will obtain figure 2.2.

On the other hand diamagnetic materials have a negative susceptibility ($\chi < 0$) and weakly repel an applied magnetic field. χ is dimensionless quantity and called as magnetic susceptibility.

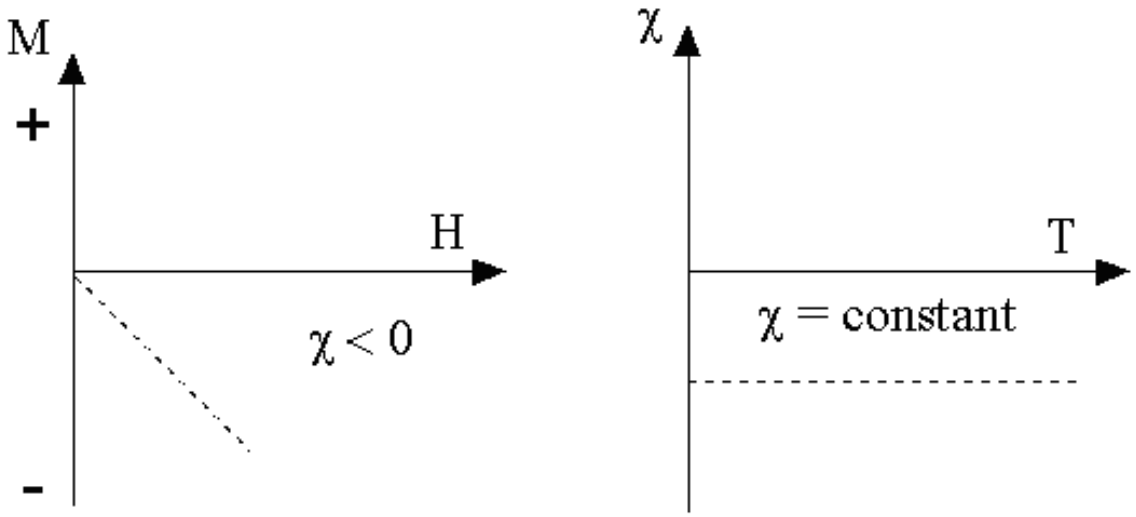

Figure 2.2 Plot of magnetization versus magnetic field strength and susceptibility versus absolute temperature for a diamagnetic material [33].

In the special case that the magnetization **M** is linearly related to the magnetic field **H**,

So from the slope of a magnetization- magnetic field graph, we find magnetic susceptibility and write the Eq. 2.2 as follows

$$M=\chi H \tag{2.2}$$

Note that when the field is zero the magnetization is zero. The other characteristic behavior of diamagnetic materials is that the susceptibility is independent from temperature.

All materials are inherently diamagnetic, but if the atoms have some net magnetic moment as in paramagnetic materials, or if there is atomic magnetic moments as in ferromagnetic materials, these stronger effects are long-range ordering which are always dominant.

2.1.2 Paramagnetism

In a paramagnet, the magnetic moments tend to be randomly orientated due to thermal fluctuations when there is no magnetic field. In an applied magnetic field these moments start to align parallel to the field such that the magnetization of the material is proportional to the applied field. On the other hand, materials whose atomic magnetic moments are uncoupled display paramagnetism independently on each atomic dipole. Hence, there is no long-range order and there is a small positive magnetic susceptibility ($\chi < 0$).

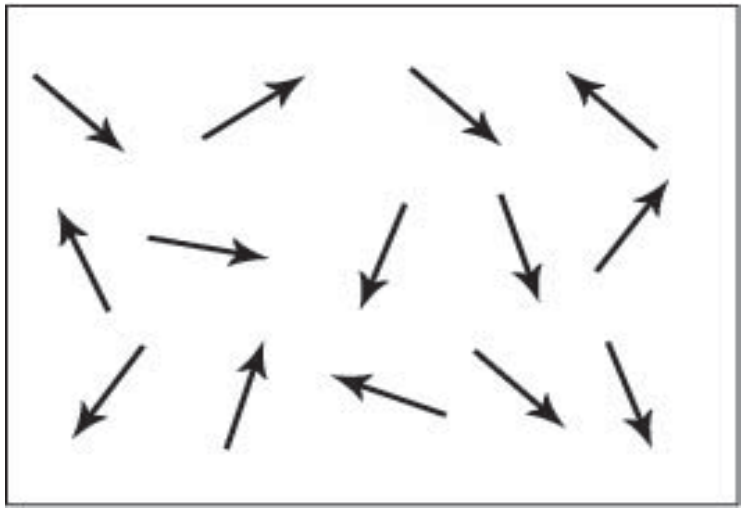

Figure 2.3 Schematic illustration of the magnetic dipole moments randomly aligned in a paramagnetic sample [34].

If we plot M vs H, and χ vs T, we will obtain figure 2.4.

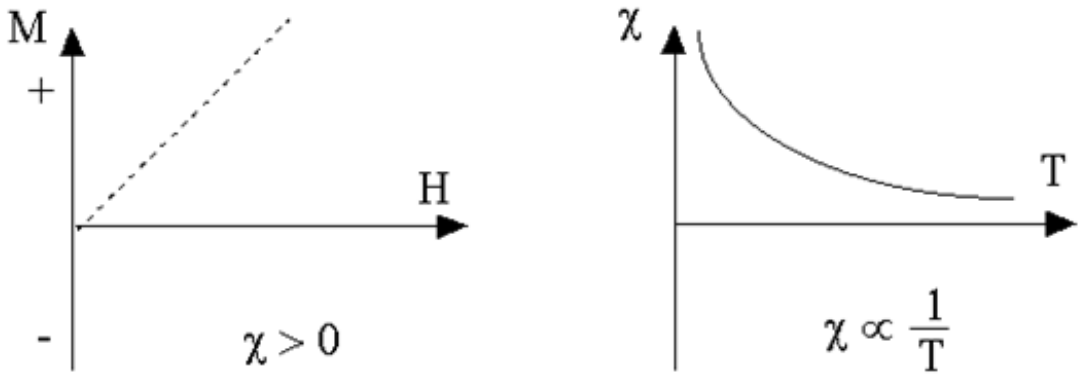

Figure 2.4 Plot of magnetization versus magnetic field strength and magnetic susceptibility versus absolute temperature for a paramagnetic material [33].

Note that magnetization is directly proportional to magnetic field strength, it can be expressed Eq. 2.2 and susceptibility is inversely proportional to the absolute temperature for a paramagnetic material.

2.1.3 Ferromagnetism

A ferromagnetic material has unpaired electrons. However, in addition to the electrons' intrinsic magnetic moments which have tendency to become aligned parallel to each other under the influence of a magnetic field. Thus, when the applied field is removed, the electrons in the material can keep each other continually pointed in the same direction.

In another word, the ferromagnetic materials exhibit parallel alignment of moments resulting in large net magnetization even in the absence of a magnetic field. We can say that the spontaneous magnetization exists inside a uniformly magnetized microscopic volume in the absence of a field. The magnitude of this magnetization, at 0 K, is dependent on the spin magnetic moments of electrons. A related term is the saturation magnetization which it can be measured in the laboratory. The saturation magnetization is the maximum induced magnetic moment that can be obtained in a magnetic field $\mathbf{H_{sat}}$ beyond this field no further increase in magnetization occurs. We can compare spontaneous magnetization with the saturation

magnetization. The saturation magnetization has to do with magnetic domains (more about domains later). Saturation magnetization is an intrinsic property, independent of particle size but dependent on temperature. When we consider figure 2.5, we can obviously understand magnetization relationship with magnetic field strength for a ferromagnetic material.

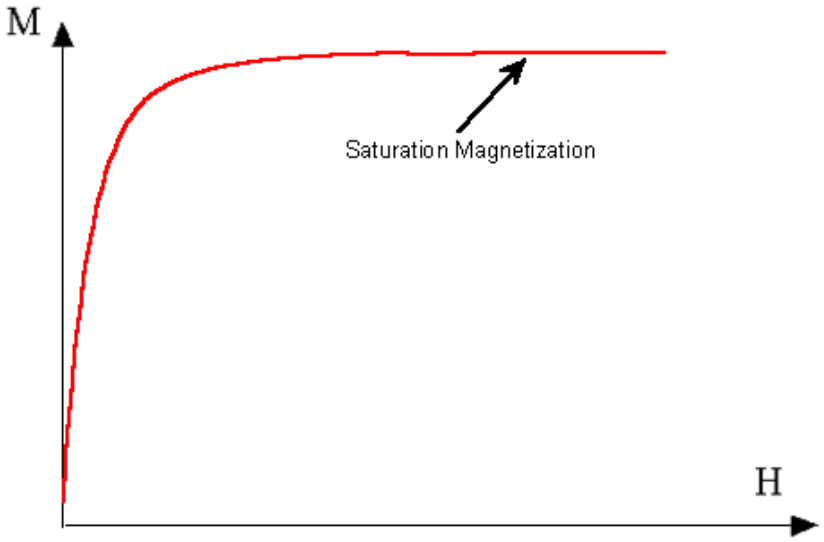

Figure 2.5 Plot of magnetization versus magnetic field strength for a, ferromagnetic material.

As compared to paramagnetic materials' magnetization between ferromagnetic materials' magnetization, there is a big difference between paramagnetic and ferromagnetic susceptibility. Therefore the magnetization in ferromagnetic materials is saturated in moderate magnetic fields and at high (room-temperature) temperatures. Every ferromagnetic material has its own individual temperature, called the Curie temperature $\mathbf{T_c}$ or Curie point, above which it loses its ferromagnetic properties. When the temperature of ferromagnetic material reaches the Curie temperature, the material loses its spontaneous magnetization and becomes paramagnetic. In a broad sense we can say that below the Curie temperature , the magnetic moments are aligned and the material is ferromagnetic. Above the Curie temperature, the thermal energy is large enough to cause a random orientation of magnetic moment, it can be disordered, hence the material becomes paramagnetic [35]. The saturation magnetization goes to zero at the Curie temperature. The Curie temperature is also an intrinsic property and is a

diagnostic parameter that can be used for mineral identification. However, it is not foolproof because different magnetic minerals, in principle, can have the same Curie temperature [33].

In addition to the Curie temperature and saturation magnetization, ferromagnets can retain a memory of an applied field once it is removed. This behavior is called hysteresis. We can say that magnetic hysteresis is an important phenomenon and refers to the irreversibility of the magnetization and demagnetization process. When a material shows a degree of irreversibility it is known as hysteretic. I will now explain the physics behind ferromagnetic hysteresis. Firstly we see a plot of the variation of magnetization with magnetic field which is called a hysteresis loop in figure 2.6.

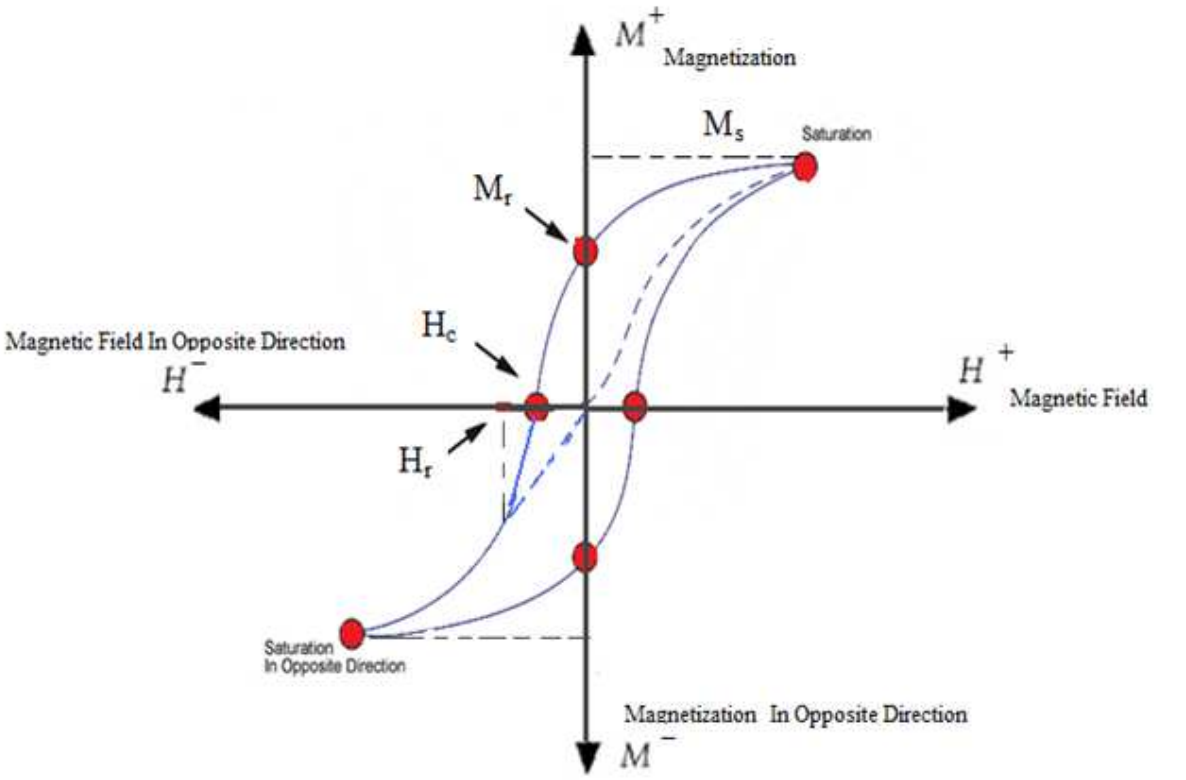

Figure 2.6 Hysteresis curve for a magnetic material [33].

According to figure 2.6 the saturation magnetization (Ms) is measured in the laboratory by applying a magnetic field. This field strength is usually sufficient to saturate most magnetic minerals. Upon reducing the field to zero, the magnetization does not go to zero but persists indicating a remanence (Mr). Increasing the magnetic field in the negative direction, a point is reached where the induced magnetization becomes zero. The field at this

point is called the coercivity (Hc). Increasing the field further in the negative direction, results in saturation again but in the negative direction. Another hysteresis property is the coercivity of remanence (Hr). This is the reverse field which, when applied and then removed, reduces the saturation remanence to zero. It is always larger than the coercive force [33].

The effect of magnetic hysteresis shows that the magnetization process of a ferromagnetic core and therefore the flux density depends on which part of the curve the ferromagnetic core is magnetized on as this depends upon the circuits past history giving the core a form of memory. Then ferromagnetic materials have memory because they remain magnetized after the external magnetic field has been removed. However, in figure 2.7**,** materials characterized by wide hysteresis loops are called hard magnetic materials. These materials cannot be easy demagnetized. Hard ferromagnetic materials are used in the fabrication of permanent magnets for motors and generators. Soft ferromagnetic materials such as iron or silicon steel have very narrow magnetic hysteresis loops resulting in very small amounts of residual magnetism making them ideal for use in relays and solenoids as they can be easily magnetized and demagnetized.

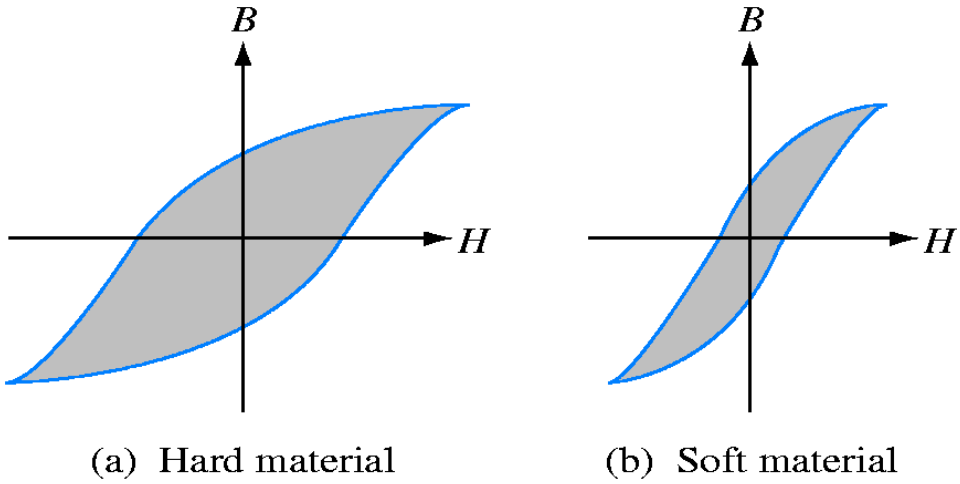

Figure 2.7 Magnetic Hysteresis loops for hard and soft materials [32].

Hysteresis results in the dissipation of energy in the form of heat with the energy wasted being in proportion to the area of the magnetic hysteresis loop. As mentioned previously, the shape of the hysteresis loop depends upon the nature of the iron or steel used and in the case of iron which is subjected to massive reversals of magnetism, for example transformer cores, it is important that the B-H hysteresis loop is as small as possible [36].

Now, I will discuss other properties of ferromagnetic materials, we know that all ferromagnetic materials contain microscopic regions called magnetic domains within which all magnetic moments aligned. These domain have volumes of about 10^{-12} to 10^{-8} m^3 and contain 10^7 to 10^{21} atoms [37].

The alignment direction differs however from one domain to another. The direction of alignment of the magnetic moments is normally along one of the crystal axes but the domains may be oriented randomly in three directions, and a single crystal may contain many domains. A magnetized domain of a material is a microscopic region within which the magnetic moments of all its atoms are aligned parallel to each other .The main implication of the domains is that there is already a high degree of magnetization in ferromagnetic materials within individual domains, but that in the absence of external magnetic fields those domains are randomly oriented. A modest applied magnetic field can cause a larger degree of alignment of the magnetic moments with the external field, giving a large multiplication of the applied field. The domains are conceptual only and not meant to give an accurate scale of the size or shapes of domains. The microscopic evidence about magnetization indicates that the net magnetization of ferromagnetic materials in response to an external magnetic field may actually occur more by the growth of the domains parallel to the applied field at the expense of other domains rather than the reorientation of the domains themselves as implied in the sketch [38].

In the absence of an external magnetic field, the domains take on random orientations relative to each other resulting in a net magnetization of zero. Here, briefly we can say about domain walls. The domain walls forming the boundaries between adjacent domains consist of thin transition regions. The domain walls where the direction of magnetization must change and the width of domain walls is controlled by the balance of energy contributions (more about domain walls later).

2.1.4 Antiferromagnetism

Adjacent magnetic moments from the magnetic ions tend to align anti-parallel to each other without an applied field. In the simplest case, adjacent magnetic moments are equal in magnitude and opposite therefore there is no overall magnetization.Briefly, we say that the atoms have mixed paralel and anti-parallel aligned magnetic moments.

2.1.5 Ferrimagnetism

The aligned magnetic moments are not of the same size; that is to say there is more than one type of magnetic ion. An overall magnetization is produced but not all the magnetic moments may give a positive contribution to the overall magnetization

Briefly we say that;

1. Empty space: $\chi = 0$, since there is no matter to magnetize, and $\mu_r = 1$
2. Diamagnetic. χ is small and negative, and μ_r slightly less than 1
3. Paramagnetic and antiferromagnetic: χ is small and positive, and μ_r slightly greater than1.
4. Ferromagnetic and ferrimagnetic: χ and μ_r are large and positive [39, 40].

where μ_r the relative permeability of the material. It can be expressed by Eq. 2.3 as follows

$$\mu_r = 1 + \chi. \tag{2.3}$$

We focus on the atomic structure that all of the other types of magnetic behavior observed in materials are at least partially attributed to unpaired electrons in atomic shells, often in the 3d or 4f shells of each atom.

2.1.6 Superparamagnetism

Superparamagnetism is a form of magnetism, which appear in small ferromagnetic or ferrimagnetic nanoparticles. In very small nanoparticles, magnetization can randomly flip direction under the influence of temperature. The typical time between two flips is called the Néel relaxation time. In the absence of external magnetic field, when the time used to measure the magnetization of the nanoparticles is much longer than the Néel relaxation time, their magnetization appears to be in average zero : they are said to be in the superparamagnetic state. In this state, an external magnetic field is able to magnetize the nanoparticles, similarly to a paramagnet. However, their magnetic susceptibility is much larger than the one of

paramagnets [41]. We know that any ferromagnetic or ferrimagnetic material undergoes a transition to a paramagnetic state above its Curie temperature. Superparamagnetism is different from this standard transition since it occurs below the Curie temperature of the material. Superparamagnetism occurs in nanoparticles which are single-domain, i.e. composed of a single magnetic domain in figure 2.8.

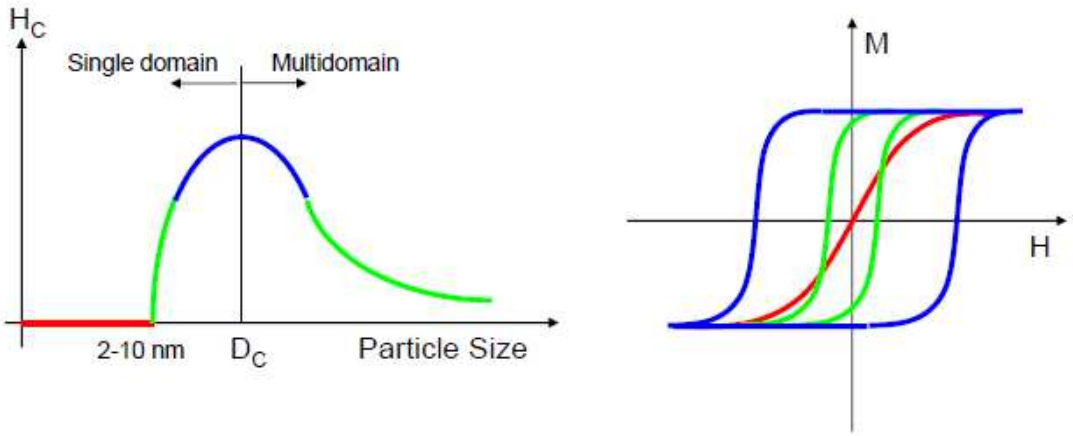

Figure 2.8 Magnetic properties of nanostructured materials [42].

when their diameter is below 3-50 nm, depending of the materials. In this condition, it is considered that the magnetization of the nanoparticles is a single giant magnetic moment, sum of all the individual magnetic moments carried by the atoms of the nanoparticle. This is what people working in the field of superparamagnetism call the "macro-spin approximation"[41].

When an external magnetic field is applied to superparamagnetic nanoparticles, they tend to align in the direction of the field via moment and particle rotation. When the field is removed the frequency of thermally activated reversals is given by

$$f = f_o e^{-\frac{E}{kT}} \tag{2.4}$$

where f_o is the "attempt frequency" which is approximately 10^9 s^{-1}. Conceptually, the frequency is the rate at which the particles approach thermal equilibrium. For relaxation times of ~100 seconds the critical energy barrier is

$$\Delta E_{crit} = \ln(tf_o)kT = 25kT \tag{2.5}$$

for thermal equilibrations. The condition for superparamagnetism is observed when a particle with uniaxial anisotropy displays zero coercive force as mathematically defined

by $KV = 25kT$ (2.6)

where K is the effective magnetic anisotropy energy constant (a function of the magnetocrystalline, shape and surface anisotropies), V is the volume of the particle and kT is the thermal energy [15,39,43]. Particles with relaxation times greater than 100 seconds or with diameters larger than the critical values are called blocked [39, 43-45]. The blocking temperature (T_B) of a material is given by

$$T_B = \frac{KV}{25k} \tag{2.7}$$

Below T_B the anisotropy of the particle blocks the free movement of the moment [15, 39]. Above the T_B the moment is free to align in an applied magnetic field and appears superparamagnetic. In an applied field at temperature T, assuming the particles' moments have achieved some level of thermal equilibrium, there will be a Boltzmann distribution of moments aligned in the direction of the applied field. This relation is essentially the case prescribed for classical paramagnetism, where the degree of orientation is given by the Langevin function

$$m_{av} = m(\coth \alpha - \frac{1}{\alpha}) \tag{2.8}$$

where $\alpha = \frac{mH}{kT}$ (2.6)

where $\mathbf{m_{av}}$ is the average magnetic moment, k is Boltzmann's constant and T is the absolute temperature [39,46]. The fundamental difference is that in the paramagnetic case the moment is a single atom, whereas now the moment considered is a single domain particle, which contains more than 105 atoms coupled ferro- or ferrimagnetically in the superparamagnetic case [39, 47]. The term superparamagnetism originates from this relation. The magnetization of an individual superparamagnetic particle is given by $M = nm_{av}$, where n is the number of

particles per volume. The defining factor between single domain and superparamagnetic particles is essentially the relaxation time relative to the experimental time. The superparamagnetic nature of the nanoparticles is derived from the randomization of aligned spins governed by Brownian motion and Néel rotation when the gradient field is removed. Brownian motion and Néel rotation are magnetic relaxation mechanisms due to particle and spin rotation, respectively. Brownian relaxation is achieved via bulk rotational diffusion of the particles in a fluid. The relaxation time for Brownian motion is given by

$$\tau_B = \frac{3V'\eta}{kT} \tag{2.7}$$

where V' is the hydrodynamic volume of the particle, η is the dynamic viscosity, k is Boltzmann's constant and T is the absolute temperature. Néel relaxation (Eq. 2.8) is attributed to the rotation of the magnetization vector or moment in the particle with a relaxation time given by

$$\tau_N = \tau_O \exp\left(\frac{\Delta E}{kT}\right) \tag{2.8}$$

where $\Delta E = KV(1-h^2)$ (2.9)

- $\boldsymbol{\tau_0}$ is a length of time, characteristic of the material, called the attempt time or attempt period (its reciprocal is called the attempt frequency); its typical value is typically estimated to be 10^{-9}-10^{-10} second.
- $\boldsymbol{\tau_N}$ is thus the average length of time that it takes for the nanoparticle magnetization to randomly flip as a result of thermal fluctuations.

$\boldsymbol{\Delta E}$ is the energy barrier assuming uniaxial on interacting particles, h is expressed as: Eq.2.10.

$$h = H/H_K \tag{2.10}$$

H/H_k is the reduced magnetic field and H_K is the internal magnetic field due to anisotropy [39,44,45].

- **K** is the nanoparticle magnetic anisotropy and **V** its volume**. KV** can be thought of as the energy barrier associated with the magnetization moving from its initial "easy axis" direction, through a "hard axis", ending at another easy axis.
- k is the Boltzmann constant.
- T is the temperature

This length of time can be anywhere from a few nanoseconds to years or much longer. In particular, it can be seen that the Néel relaxation time is a function of the exponential of the grain volume, which explains why the flipping probability becomes rapidly negligible for bulk materials or large nanoparticles.

Let us imagine that the magnetization of a single superparamagnetic nanoparticle is measured and let us call τ_m the measurement time. If $\boldsymbol{\tau_m} >> \boldsymbol{\tau_N}$, the nanoparticle magnetization will flip several times during the measurement so the magnetization measured will be zero. If $\boldsymbol{\tau_m} << \boldsymbol{\tau_N}$, its magnetization will not flip during the measurement so the magnetization measured will be the magnetic moment carried by the nanoparticle. In the former case, the nanoparticle will appear to be in the superparamagnetic state whereas in the latter case it will appear to be ferromagnetic. The state of the nanoparticle (superparamagnetic or ferromagnetic) depends on the measurement time. A transition between superparamagnetism and ferromagnetism occurs when $\boldsymbol{\tau_m} = \boldsymbol{\tau_N}$. In several experiments, the measurement time is kept constant but the temperature is varied so the transition between superparamagnetism and ferromagnetism is seen as a function of the temperature. The temperature is called blocking temperature. Above ıt was discused and formulated. Experimental conditions for superparamagnetism are:

1) relaxation times faster than the measurement times (commonly ~100 s)

2) superparamagnetic nanoparticles have a much larger susceptibility than standard paramagnets: they behave exactly as a paramagnet with a huge magnetic moment. When the magnetic field is removed, the clusters will not randomize their direction immediately, but rather it will take some length of time to do so. Larger clusters tend hold their magnetization for much longer

3) the magnetization curve does not display hysteresis .

In recent years, we know the superparamagnetic materials which have wide applications in the technological point of view. Superparamagnetism is a finite size effect since the particle anisotropy is generally proportional to its volume and has important applications in the thermal and time stability of the bits written in recording media. Spin glass property is also has some relevant applications in the memory devices [48].

2.2 Magnetism of Nanoparticles

The aligned spin arrangements in ferromagnetic, antiferromagnetic, ferrimagnetic and superparamagnetic materials are subdivided into regions throughout the bulk material. Previous section the region was called magnetic domain. I give more detail about magnetic domain. When the material is demagnetized the vector summation of all the magnetic moments from all the domains equals zero. When the material is magnetized the vector summation of the magnetic moments gives an overall magnetic moment. Now we can ask a question that Why do domains occur in materials? The exchange interaction it would appear that the most stable state would be that of a single domain where all electron spins would be aligned parallel. However, while this minimizes the energy contribution arising from the exchange interaction, there are other contributions to the total magnetic energy that must be considered: Magnetostatic energy, Magnetostrictive energy and Magnetocrystalline energy. We will explain each one.

Magnetostatic energy: If a material consists of a single domain then it behaves as a block magnet in figure 2.9 (i) and so a "demagnetising field" (the blue arrows) must be present around the block. This external, demagnetising field has a magnetostatic energy that depends on the shape of the sample and is the field that allows work to be done by the magnetized sample. In order to minimize the total magnetic energy the magnetostatic energy must be minimised. This can be achieved by decreasing the external demagnetising field by dividing the material into domains in figure 2.9 (ii). Adding extra domains increases the exchange energy, as the domains cannot align parallel, however the total energy has been decreased as the magnetostatic energy is the dominant effect. The magnetostatic energy can be reduced to zero by a domain structure that leaves no external demagnetizing field in figure 2.9.

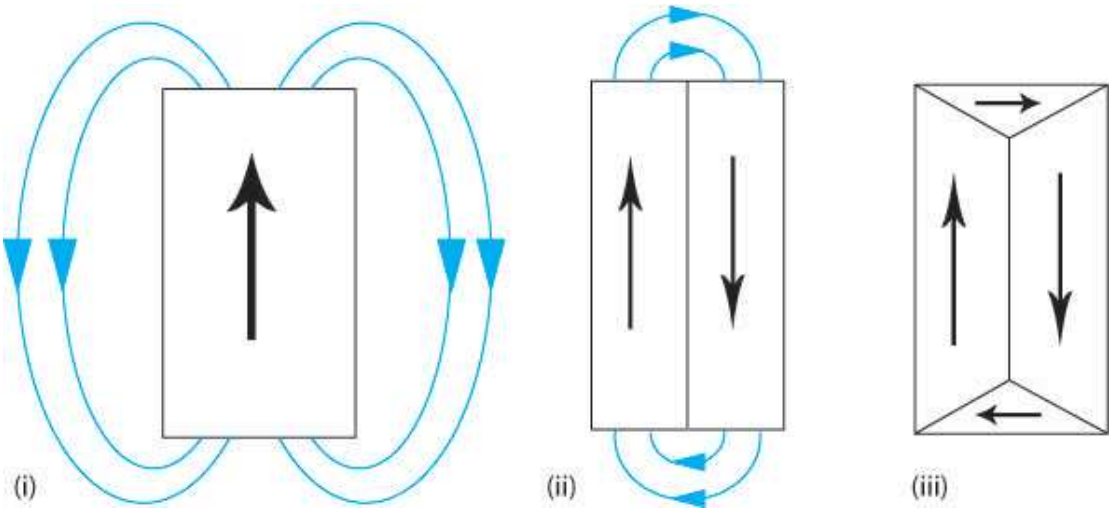

Figure 2.9 Schematic illustration of how the addition of domains can reduce the external demagnetizing field, therefore, reducing the magnetostatic energy [34].

This is the main driving force for the formation of domains.

Magnetocrystalline energy: Up until now, we have ignored the influence of the atomic lattice structure; however this also has an affect on the total energy of a magnetized sample. A ferromagnetic material has *'easy'* crystallographic directions along which it is preferred that the magnetisation vector points and 'hard' directions along which a higher field is required to achieve the same magnetisation. Therefore, it is easiest to magnetize a ferromagnetic material along these easy axes, as shown by the schematic below.

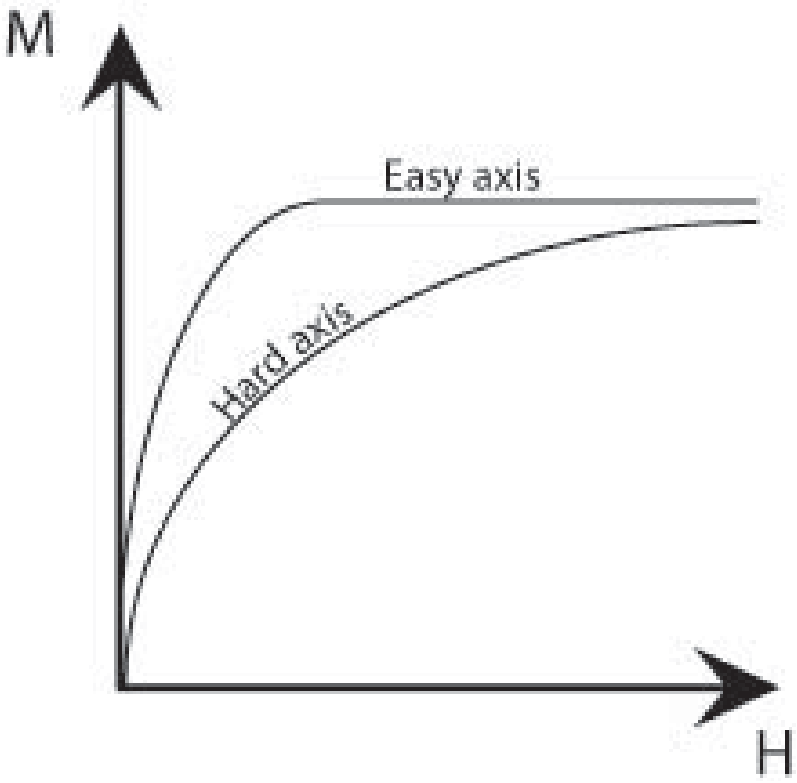

Figure 2.10 Schematic illustration of the difference in size of field required to achieve the same magnetisation a long easy and hard axes [34].

There is an energy difference associated with magnetisation along the hard and easy axes which is given by the difference in the areas under **(M, H)** curves. This is called the magnetocrystalline energy. This energy can be minimized by forming domains such that their magnetisations point along the easy crystallographic directions. The ideal material might have easy crystallographic directions perpendicular to one another as then both the magnetostatic and magnetocrystalline energies could both be minimized in figure 2.9 above. In the regions bounding the domains, the domain walls, there must be a change in the direction of the magnetization. Therefore, it cannot be aligned along easy axes and so large domains with few domain walls minimize the magnetocrystalline energy.

Magnetostrictive energy: When a ferromagnetic material is magnetized it changes length. This is known as magnetostriction; an increase in length along the direction of magnetisation is positive magnetostriction like this Fe, and a decrease in length is negative magnetostriction like this Ni. These length changes are usually extremely small; in the range of tens of parts per million. However, they do affect the domain structure of the material. It is impossible for

both to be accommodated and so this causes elastic strain in the material. The elastic strain energy is proportional to the volume of the domains of closure hence magnetostrictive energy can be minimized by decreasing the size of these domains. Reducing the volume of the domains of closure also requires the primary domains to decrease in size and increase in number. The addition of extra domain walls increases the magnetocrystalline and exchange energy contributions to the total energy. The actual domain structure is a compromise of all the mentioned energy contributions. Now, we focus on concept of domain wall. Domain walls are the regions between domains where the direction of magnetisation must change, usually by either 180° or 90° in figure 2.11.

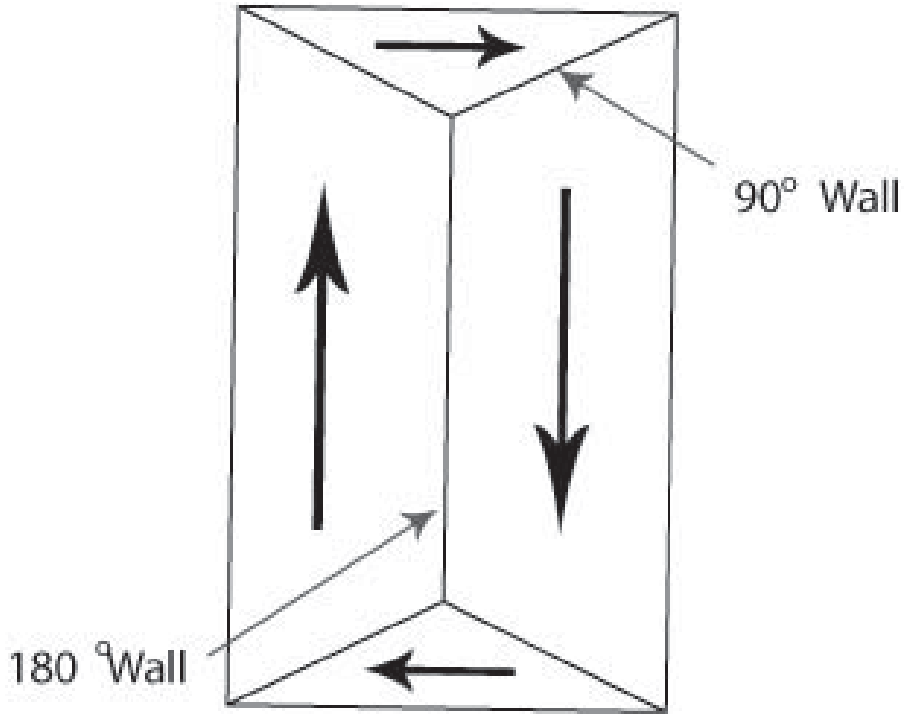

Figure 2.11 Diagram illustration of domain walls [34].

The width of domain walls is controlled by the balance of two energy contributions: Exchange energy, magnetocrystalline energy .The exchange energy favors wide walls where adjacent magnetic dipole moments can be as close to parallel as possible, whereas the magnetocrystalline energy favor sharp changes in the dipole moments between the favored directions in the crystal so that as few dipole moments as possible point along “non-easy”

directions. The actual width is determined by the minimum of the total energy. The most favorable domain walls are those which do not require an external demagnetising field. Consequently, below this size a ferromagnetic material exists as a single-domain particle. This means that the particle is in a state of uniform magnetization. The constituent spins, at temperatures well below the Curie temperature, rotate in unison. The exchange energy is strong enough to hold all spins tightly parallel to each other and determines the value of the particle magnetic moment, while its direction is determined by the total anisotropy energy. The typical size of a single-domain particle is in the order of a few tens of nanometers depending on the material and contributions from various anisotropy energy terms. Therefore, it can be concluded that single domain particles are in general not isotropic, but they will have anisotropic contributions to their total energy associated with their external shape, the magneto-crystalline structure itself and the imposed stress. This anisotropic behavior of single-domain particles will be discussed below.

In principle, single-domain particles must reverse their magnetization by coherent spin rotation. This is a comparatively difficult process, if the particle has a significant magnetic anisotropy. Consequently, single-domain particles are expected have a high coercivity, which is the basis of most of their applications. This (non thermal) magnetization reversal mechanism was first studied by Stoner and Wohlfarth in 1948 [39, 49]. Neel predicted that at nonzero temperature the magnetization can overcome the energy barrier as a result of thermal agitation [39, 50]. Later, Brown derived the Fokker-Planck equation for the probability distribution of spin orientations, starting from the stochastic Landau-Lifshitz equation, and calculated approximate expression for the relaxation time of particles with uniaxial anisotropy [39, 51]. The theoretically most well studied systems are noninteracting classical spins representing the magnetization of the nanoparticles with axially symmetric magnetic anisotropy.

2.3 Superparamagnetic Resonance

Magnetic properties of superparamagnetic nanoparticles can be measured by various methods. One of them is Electron Spin Resonance (ESR) technique which is called as Superparamagnetic Resonance (SPR). This method can be described as follows.

2.3.1 Magnetic Susceptibility

A correlation between the resonance magnetic field and the peak to peak line width is often observed in low temperature superparamagnetic resonance (SPR) studies of fine magnetic nanoparticles. In order to account for this correlation, we considered the resonance line shapes resulting from Landau-Lifshitz equation for the analysis of the data [52- 54].

$$M' = \gamma M \times B_{eff} + \frac{\lambda}{M^2} M \times (M \times B_{eff}) \tag{2.11}$$

Especially in numerical computer simulation of SPR spectra and in theoretical modeling, at different low temperature regions, the resonance line broadening should be treated separately from the distribution of resonance magnetic field. The resonance field and line width of the SPR spectra were analyzed in this study. At low temperature the resonance of the individual magnetic particles occurs with a considerable line width. The dynamic susceptibility is given by $\chi = \chi_1 - i\chi_2$ where χ_1 and χ_2 are the real and imaginary parts of the susceptibility, respectively. The microwave absorption is proportional to the imaginary part of the dynamic susceptibility.

$$\frac{dP}{dB} \propto \frac{d\chi_2}{dB} \tag{2.12}$$

dB And, therefore the following individual line shape is obtained [52- 54].

$$\chi_2 = \frac{1}{\pi} \frac{B_0^2 \Delta_B [(B_0^2 + \Delta_B^2) B^2 + B_0^4]}{[B_0^2 (B - B_0)^2 + \Delta_B^2 B^2][B_0^2 (B + B_0)^2 + \Delta_B^2 B^2]} \tag{2.13}$$

Here we defined

$$B_0 = -\omega / \gamma \tag{2.14}$$

As the resonance magnetic field and the line width,

$$\Delta_B = \lambda B_0 / |\gamma| |M_0| \tag{2.15}$$

2.3.2 Resonance Field

The analytical expression for the apparent resonance-field shift has been obtained. Computer simulations using the derivative magnetic susceptibility provide good fits of the resonance spectra at different temperatures for the same magnetic and morphological parameters of the particles. In contrast to Lorentzian (or Gaussian), the line shape of Eq. 2.16 is characterized by an apparent resonance field (that at the maximum of resonance absorption) depending on the line width given by [20, 53, 54].

$$B_r = \frac{B_0^2}{B_0^2 + \Delta_B^2} [2B_0 (B_0^2 + \Delta_B^2)^{1/2} - B_0^2 - \Delta_B^2]^{1/2} \tag{2.16}$$

2.3.3 SPR Line Width

In a recent investigation on the SPR of nanoparticles at different temperatures [20, 53-55] it has been shown that the individual line width for the SPR of nanoparticles at different temperatures can be well fitted by

$$\Delta_B = \Delta_T L(x) \tag{2.17}$$

In this equation Δ_T is a saturation line width at a temperature T,

$$L(x) = \coth x - 1/x \quad \text{is the Langevin function with} \tag{2.18}$$

$$x = M_S V B_{eff} / k_B T \tag{2.19}$$

V is being the particle volume. Besides, the thermal fluctuation-induced modulation of the magnetocrystalline anisotropy energy has been taken into account to describe the rapid increase of the individual line width by decreasing the temperature. This mechanism leads to a temperature dependence of Δ_T. The resulting volume and temperature dependence of the individual line width is then [20, 53- 55];

$$\Delta_B = \Delta_0 L(x) G(y) \tag{2.20}$$

Where Δ_0 is the saturation line width at 0 K and G(y) is the superparamagnetic averaging factor given as:

$$G(y) = \frac{1}{L(y)} - \frac{10}{y} + \frac{35}{y^2 L(y)} - \frac{105}{y^3} \tag{2.21}$$

With $$y = K_1 V_S / kT \tag{2.22}$$

where K_1 is the first order magnetocrystalline anisotropy constant and V_s is the reference volume (presumably the greatest volume in the statistical ensemble). The magnetic parameters of zinc ferrite ($ZnFe_2O_4$) nanoparticles have been used in the simulations. The best fit values of the adjustable simulation parameters have been determined.

Note that one and the same set of these parameters provides the best fits to the spectra recorded in the whole temperature range of this study.

CHAPTER 3

GENERAL PROPERTIES OF $ZnFe_2O_4$ AND $Co_{0.3}Zn_{0.7}Fe_2O_4$

In this chapter we will examine the molecular properties of $ZnFe_2O_4$ and $Co_{0.3}$ $Zn_{0.7}Fe_2O_4$ nanoparticles. I will also discuss spinel structure.

3.1 Properties of $ZnFe_2O_4$

Recent experimental studies on nanocrystalline $ZnFe_2O_4$ have suggested that the cation distribution in this material is partially inverted and this gives rise to scope for potential technological applications [56,57]. Inview of this a considerable amount of research has been done to investigate the effect of grain size onthe cation distribution and magnetic properties of nanocrystalline $ZnFe_2O_4$. All these studies agree in one aspect that $ZnFe_2O_4$ is magnetically ordered with high ordering temperature and large magnetic moment. But they differ in predicting the type of magnetic ordering [56, 58-62]. In order to confirm the typeof magnetic ordering and to study the effect of grain boundary and surface spins on the magneticproperties of nanostructured $ZnFe_2O_4$.

Recent investigations of spinel ferrites have repeatedly shown this rich variety of magnetic ordering that ranges from classical ferrimagnetic ordering to spin glass behaviour. The magnetic behaviour of the particle surface differs from that corresponding to the core, because of the distinct atomic coordination, compositional gradients and, concentration and nature of the defects present in both the regions. Thus, whereas the core usually displays a spin arrangement similar to that of the bulk material, a much higher magnetic disorder is

present in the surface, giving rise to magnetic behaviour which covers from that of a dead magnetic layer to that of a spin-glass like [48].

In recent years, $ZnFe_2O_4$ nanoparticles prepared using varied methods, such as traditional ceramic synthesis [14, 30], aero-gel procedure [14, 26, 29, 31, 63-65], low-temperature hydroxide co-precipitation and hydrothermal synthesis [14, 66, 67], have been studied and observed to be ferrimagnetic or superparamagnetic.

We focus on molecular structure of $ZnFe_2O_4$, the ferrite is called a normal spinel. Normal spinel ´s crystal structure can show in figure 3.1.

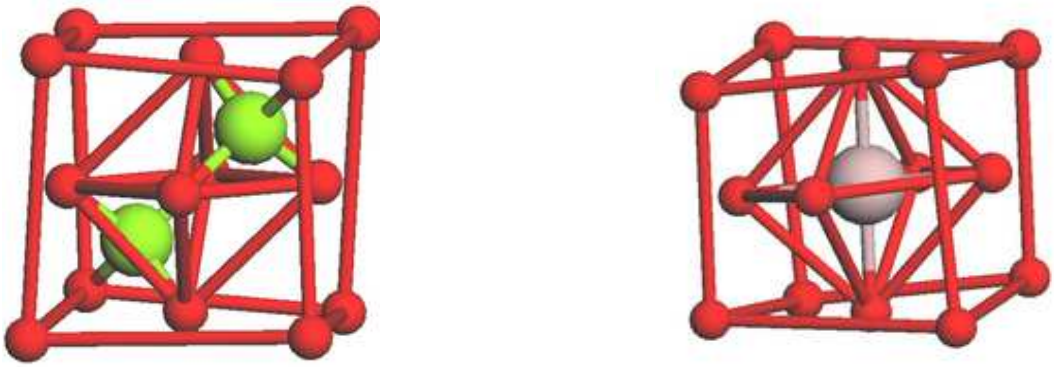

(i) (ii)

Figure 3.1 Normal spinel structure [68].

According to figure 3.1 (i) two kinds of occupied tetrahedral sites in spinel sub-cell a. A is in green , O is in red and figure 3.1(ii) occupied octahedral site in spinel sub-cell b. B is in gray, and O is in red.It can be formülated AB_2O_4 Spinel .We can show $ZnFe_2O_4$ normal spinels.It can be expressed as in (3.1).

$$[Zn]^{tet}\,[Fe_2]^{oct}O_4 \qquad (3.1)$$

It crystallizes in the spinel structure which contains two different cation sites. There are eight tetrahedral A sites and 16 octahedral B site in $ZnFe_2O_4$ nanocrystals. Magnetic coupling occurs via super exchange. The A-A and B-B couplings are weak compared to the

A-B interaction. In a normal spinel all Zn atoms are on A sites, all Fe atoms on B sites. In a fully inverse spinel the Zn atoms occupy half of the B sites, while half of the Fe atoms rest on A sites, the other half on B sites [48].

The systems where one or both the sublattices are populated with magnetic ions, the competing exchange interactions may lead to topological frustration, yielding a magnetic structure that may include states of antiferromagnetic order, local spin canting, spin glass behaviour, disordered phases and ferromagnetic order. In 1961, Neél suggested that small antiferromagnetic particles can exhibit super-paramagnetism and weak ferromagnetism due to uncompensated spins in the two sublattices [14, 65].

3 .2 Properties of $Co_{0.3}\,Zn_{0.7}\,Fe_2O_4$

Studies of spinel ferrites are highly relevant to modern technologies, so the synthesis and sintering of ferrites have become an important part of modern ceramic research [69-72].Spinel ferrite systems have got excellent oppornities for understanding and finetuningthe superparamagnetic properties of nanoparticles by reason of the rich crystalchemistry [73,74].Cobalt-zinc ferrite is one of the soft ferrites used in electronic devices such as transformer cores, electric motors and generators. In its applications, it is subjected to alternating magnetic fields, and should therefore present low energy losses [69,71,75,76].

We focus on molecular structure of Co-Zinc ferrite. It can be expressed as in (3.2).

$$Co_{(1-x)}\,Zn_xFe_2O_4 \tag{3.2}$$

for X =0.7 and it can be represented by $Co_{0.3}\,Zn_{0.7}\,Fe_2O_4$. The distribution of the cations in Co-Zinc ferrite, ıt can be can be expressed as: (3.3)

$$Zn^{2+}{}_x\,Fe^{3+}{}_{1-x}\,[Co^{2+}{}_{1-x}\,Fe^{3+}{}_{1+x}\,]\,O_4 \text{ [69,77-79] .} \tag{3.3}$$

The substitution of Zn^{2+} for Fe^{3+} reduces the Curie temperature of the ferrite [69,77,78,80] On the other hand, increasing the zinc content of cobalt-zinc ferrites increases

their lattice parameter [69,81-83]. While decreasing the saturation magnetization due to augmented B-B interaction followed by reduced A-B interaction. Also, the presence of Co^{2+} ion in the cobalt-zinc ferrite hastens the $Co^{2+} + Fe^{3+} \Leftrightarrow Co^{3+} + Fe^{2+}$ exchange reaction in octahedral sites, while tetrahedral sites are preferentially occupied by zinc cations.

This exchange reaction supports the electronic conduction mechanism in cobalt-zinc ferrites [69, 83, 84]; the octahedral sites become enlarged when they are occupied by Fe^{2+} ions instead of Co^{2+} ions [69, 77, 79, 85].

CHAPTER 4

EXPERIMENTAL

4.1 Synthesis and Characterization of $ZnFe_2O_4$ Nanoparticles

All reagents were used as received, without further purification. In an appropriate ratio, analytical grade of zinc nitrate [$Zn(NO_3)_2.6H_2O_4$] and constant amount of ferric nitrate [$Fe(NO_3)_2.\ 9H_2O_4$] and urea (1g) were mixed to obtain precursor solution of $ZnFe_2O_4$. The crucible containing the solution was introduced into a microwave oven. Initially, the solution boils and undergoes dehydration followed by decomposition with the evolution of large amount of gases (N_2, NO_2, CO_2). After the solution reaches to the point of spontaneous combustion, it begins to burn and releases lots of heat, vaporizes all the solution instantly and becomes solid burning at the temperature over 1000^{o}C. The entire combustion process takes only 5 min to produce ferrite powders in a microwave oven.

The structural characterization of the as synthesized $ZnFe_2O_4$ was done by X-Ray powder diffraction method. The broad peaks in the XRD pattern suggested the nanocrystalline nature of the product. All the diffraction peaks were indexed to the cubic structured $ZnFe_2O_4$ with cell constant a = 8.434±0.02 A°, which is good agreement with the value in the literature (JCPDS card no. 89-1012, with a = 8.433 A°). The average crystallite size, L, was estimated by the Scherrer equation from the X-ray peak broadening (full-width at half maximum, FWHM) of the most intense peak (3 1 1). Crystallite size of synthesized $ZnFe_2O_4$ powder, based on this equation, was calculated as ~41nm [14, 73].

4.2 Synthesis and Characterization of $Co_{0.3}Zn_{0.7}Fe_2O_4$ Nanoparticles

All the reagents were used without further purification. The $Co_{0.3}Zn_{0.7}Fe_2O_4$ nanoparticles were elaborated by using a hydrothermal route. In a typical experiment, stoichiometric amount of metal chlorides were completely dissolved in 20 ml distilled water by stirring. Then 30 g PEG-400, heated and melted, was added to above mixture, followed by addition a certain amount of NaOH until the pH of the solution reached to 11. After continuous stirring for an hour, a homogeneous solution could be obtained. The mixed solution was poured into a Teflon lined stainless-steel autoclave (60 ml) with a filling degree of 60 %. The autoclave was kept at 150^{o}C temperatures for 12 h, and then it is cooled to room temperature naturally. The products were filtered and washed several times with distilled water and absolute ethanol, and finally, dried in a vacuum oven at 70^{o}C for 6 h. [14, 73].

The structural characterization of the as synthesized $Co_{0.3}Zn_{0.7}Fe_2O_4$ was done by X-Ray powder diffraction method. The broad peaks in the XRD pattern suggested the nanocrystalline nature of the product. All the diffraction peaks were indexed to the cubic structured $Co_{0.3}Zn_{0.7}Fe_2O_4$ with cell constant a = 8,424±0.02 A°, which is good agreement with the value in the literature (JCPDS card no. 89-1012, with a = 8,424 A°). The average crystallite size, L, was estimated by the Scherrer equation from the X-ray peak broadening (full-width at half maximum, FWHM) of the most intense peak (3 1 1). Crystallite size of synthesized $Co_{0.3}Zn_{0.7}Fe_2O_4$ powder, based on this equation, was calculated as ~9.4 nm [14, 73].

4.3 Superparamagnetic Resonance Measurements

The magnetic properties of polycrystalline powders of superparamagnetic zinc ferrite ($ZnFe_2O_4$) nanoparticles were investigated by conventional X-band (f @ 9.5 GHz) Bruker EMX model spectrometer employing an ac magnetic field (100 kHz) modulation technique and the first derivative absorption signal at different temperatures were recorded figure 4.1.

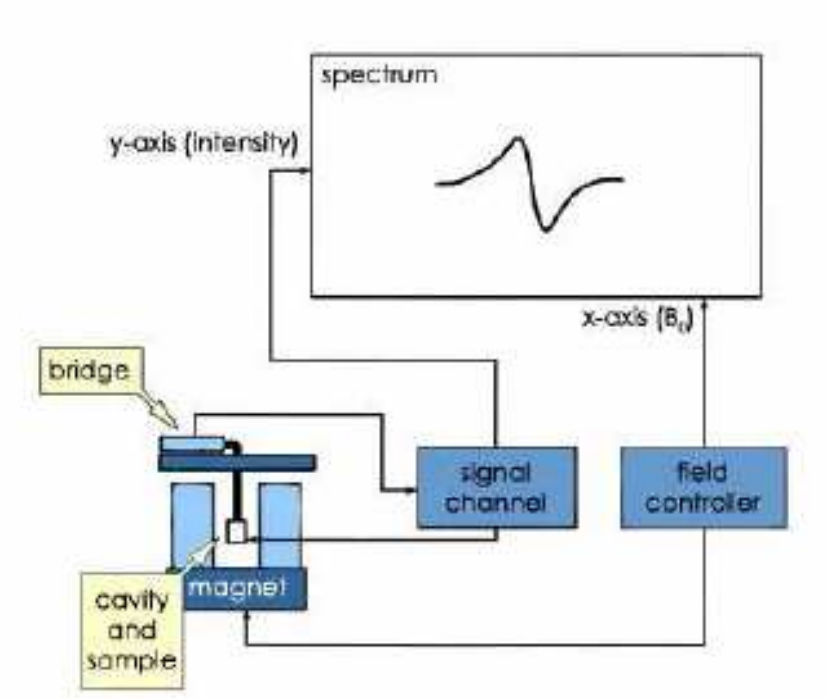

Figure 4.1 Block diagram of an ESR spectrometer [39].

Operating conditions were 0.20 mW microwave power, 20 G modulation amplitude, center field 3500 G, sweep width 5000 G, time constant 40.96 s and sweep time 41.94 s with multiple accumulations to enhance the signal-to-noise ratio. An Oxford continuous helium gas flow cryostat has been used, allowing the X-band microwave cavity to remain at ambient temperature during ESR measurements at low temperatures. The temperature was stabilized by a conventional Lakeshore 340 temperature controller within an accuracy of 1 degree between 10 and 300 K. The field derivative of microwave power absorption, dP/dH, was registered as a function of DC magnetic field H. To obtain the intensity of the microwave power absorption, P, digital integration of the EPR curves was performed by using Bruker WinEPR software.

N-Diphenyl-N'-(2, 4, 6-trinitrophenyl)-hydrazyl (DPPH) was used for as a standard g-marker which has small and narrow peak corresponding g=2.0036.

CHAPTER 5

RESULTS AND DISCUSSION

In this chapter the results obtained from the experiments and the discussions on these results are given for $ZnFe_2O_4$ and $Co_{0.3}Zn_{0.7}Fe_2O_4$ nanoparticles. The original SPR absorption spectra for some chosen temperatures are illustrated and the temperature variations of the line width, the resonance field and the SPR signal intensity will be discussed in the following subsections.

5.1 Sample: $ZnFe_2O_4$

In this work temperature dependent magnetic properties of $ZnFe_2O_4$ nanoparticles synthesized by PEG assisted hydrothermal method were investigated by superparamagnetic resonance (SPR) technique by using conventional X-band (f @ 9.5 GHz) Bruker EMX model spectrometer .The first derivative of microwave power absorbed by the sample with respect to the static magnetic field, *dP/dH,* is plotted as a function of static field for some selected temperatures as shown in Figure 5.1.

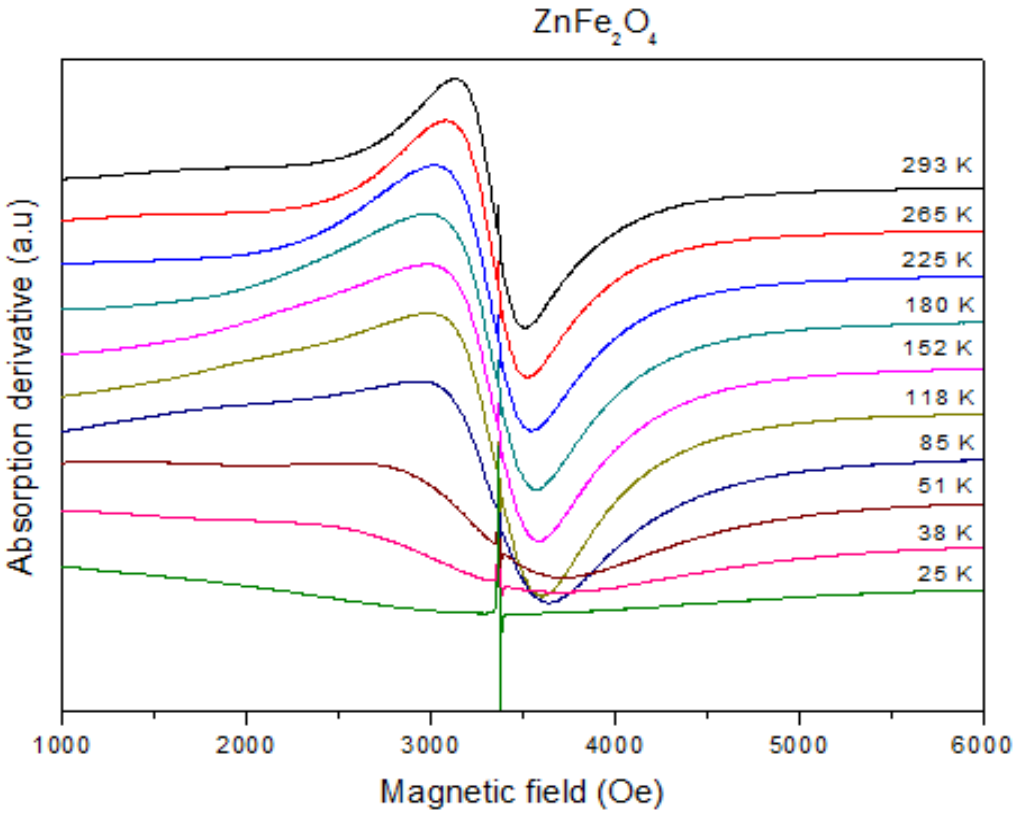

Figure 5.1 SPR spectra as a function of temperature. Solid lines are SPR fit.

As it is seen from this figure, the resonance field and the line width of the SPR spectra are strictly temperature dependent. At room temperature, a single, strong and broad SPR signal was observed with the resonance field and the line width of 3316 G and 382 G, respectively. The sample can only be a superparamagnetic state at room temperature. It can be seen that the SPR signals taken from the sample are almost symmetric with respect to the resonance field (Hr) at all temperatures. Such a symmetric signal may be attributed to a single type of species. It should be noted that the signal amplitudes are given in arbitrary unit. As the temperature is decreased, the line broadens and shifts down to lower fields.

5.1.1 Linewidth

Figure 5.2 shows the temperature variation of the line width values of the SPR spectra of $ZnFe_2O_4$ nanoparticles. As seen from the figure, the line width sligthly increases as the temperature decreases down to 200 K and increases smoothly between 100 and 200 K. Then, below 100 K, a sharp increase in the line width is observed down to lowest temperature. It is known that, in a randomly oriented ferromagnet the absorption line width follows a non-monotonic function of temperature. At low temperatures the line width is large due to the scattering in direction of anisotropic field of particles (inhomogeneous broadening). As the temperature increases the tendency to make magnetic moment isotropic causes the line width to decrease.

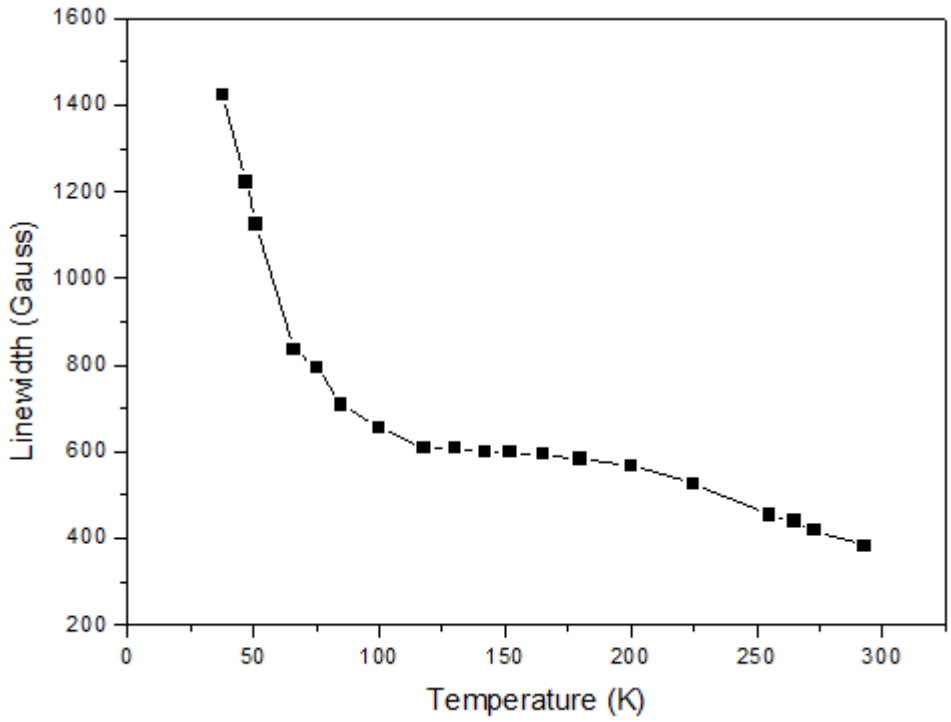

Figure 5.2 Temperature variation of SPR line width and the theoretical fit.

The smaller line width at high T is due to the smaller effective anisotropy induced by the thermal average following a superparamagnetic (SPM) behaviour. In the high-T (100 K < T < 300 K) regime the line shapes are almost symmetrical. The effective anisotropy and interactions between particles are smoothed by the thermal fluctuations [20, 52, 86].

The linewidth increases as the effective anisotropy becomes more important with decreasing temperature.

5.1.2 Resonance field

Figure 5.3 shows the variation of the resonance field values (measured from the magnetic field at the center of the SPR resonance curve) with the temperature. The figure implies that the resonance field decreases smoothly when the temperature decreases down to 100 K and it decreases slightly between 70 and 100 K. Below this temperature the resonance field decreases sharply down to 25 K. And no measurement can be done below 25 K, since the signal intensity goes to almost zero and the SPR signal is shifted to lower fields.

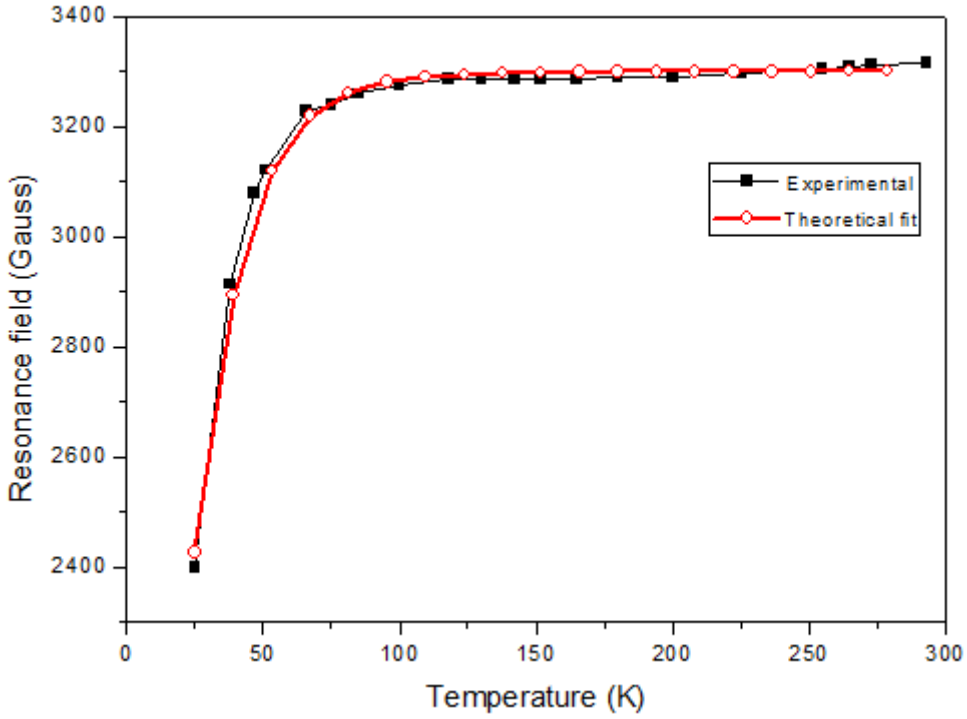

Figure 5.3 Temperature dependence of apparent SPR resonance field and the theoretical fit.

For the resonance field there arises two distinct regions (i) for T>100 K and (ii) T<100 K. The behaviour for T>100 K can be explained as follows. It is known that dependence of uniaxial anisotropy energy on temperature is similar to that of magnetostatic i.e. demagnetization [20, 87]. The decrease of resonance field for T<100K is intriguing. This behaviour can be explained on the line similar to that suggested by Kodama et al [88]. Below 100 K the surface spins freeze and they freeze in the direction of DC-magnetic field. This yield an exchange coupling between the surface and core spins. This gives rise to a 'unidirectional' anisotropy with easy axis in the direction of the field [20, 52, 87, 89]. As a result there is sudden decrease in the resonance field below 100 K [87- 89].

5.1.3 The anisotropy field

The anisotropy field values (obtained by B(290 K) – B(T)) in Fig. 5.4 are slightly increasing on decreasing the temperature to 130 K. Below this temperature, they are increasing sharply down to the lowest temperature and reach a value of 918 G. This anisotropy cannot originate from the shape of the particle, so it can be expected to originate from the particle surface and this agrees with the magnetization measurements and Monte Carlo simulations performed on the nanoparticle system [20, 54] So, the results can be interpreted by a simple model, in which each single-domain nanoparticle is considered as a core–shell system, with magneto crystalline anisotropy on the core and surface anisotropy on the shell. The surface contribution is more evident in the absence of inter-particle interactions as seen by Zysler et al [20, 90].

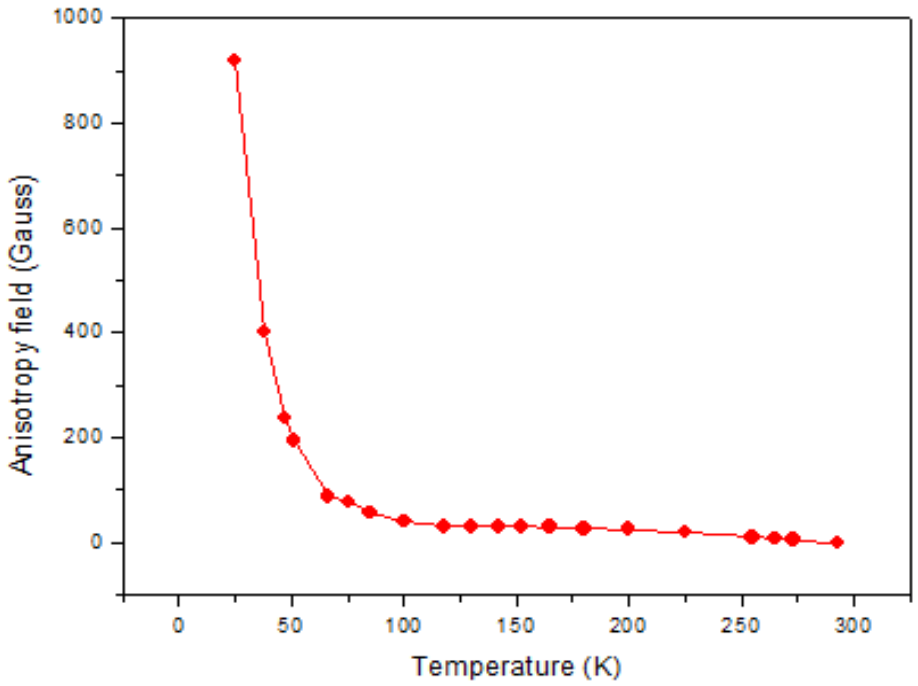

Figure 5.4 Anisotropy field values obtained by B(290 K) – B(T).

Superparamagnetic resonance experiments render information on the internal magnetic order of the nanoparticles. At high temperature, the SPR line shape is governed by the core anisotropy and the thermal fluctuations. By decreasing the temperature, as the shell spins increase their magnetic susceptibility, they produce an effective field on the core, leading to a decrease of the resonance field from its high temperature value. As the shell spins begin to order the effective anisotropy increases, following its surface value more closely.

5.1.4 The SPR intensity

Figure 5.5 shows the temperature dependence of the SPR spectra intensity obtained by double integration of the experimental derivative of absorption spectra. One can see that this dependence is quite similar to that observed for the zero field cooled (ZFC) magnetic susceptibility of $ZnFe_2O_4$ nanoparticles [20, 53, 91, 92]. A distinct maximum occurs at around 100 K.

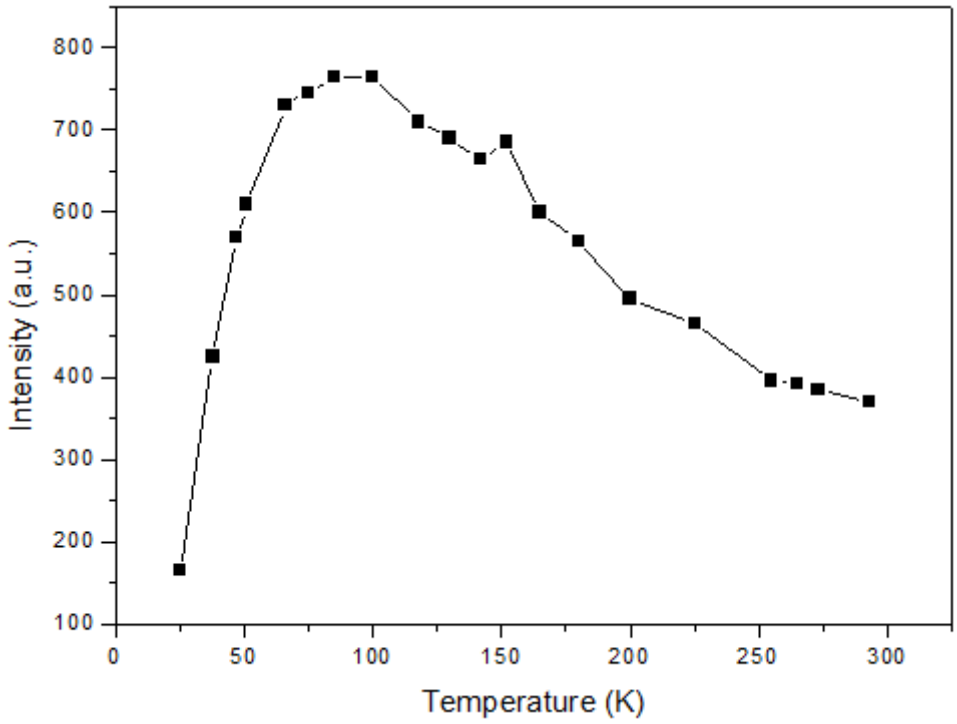

Figure 5.5 SPR intensity values obtained by double integration of signals.

An order–disorder transformation involving occupation of octahedral and tetrahedral sites by Fe^{2+} and Fe^{3+} ions takes place at this temperature. This causes a peak in the susceptibility (SPR intensity) temperature plot as seen in the present case. This transition is accompanied with a structural change from cubic to monoclinic, and is presumably a consequence of a band splitting caused by electron correlations and/or electron–phonon interactions. The crystallographic transition also results in an electrical or magnetic transition, where in the low-temperature phase the sixth 3d electron is localized, inducing a high resistivity and a low magnetization [20, 53, 91, 92].

The transition temperature for this $ZnFe_2O_4$ diluted powder is slightly higher than that of bulk. The flatness of this maximum can be related to the distribution in the blocking temperatures caused by the spread in nanoparticle sizes.

5.1.5 Summary for $ZnFe_2O_4$ nanoparticles

The SPR spectra of $ZnFe_2O_4$ nanoparticles at low temperature become very broad (with the peak to peak line width comparable to the apparent resonance field at the X-band) and shift towards lower magnetic fields. The individual nanoparticle line shapes were well

described by the Landau–Lifshitz line shape function, which accounts for both the above-mentioned features in the temperature behaviour of the spectra. We remark the existence of two behaviours, one at high and the other at low temperature. In the high-temperature regime we observed a superparamagnetic behaviour and a small anisotropy. At low temperature the experiments show signs of a high anisotropy. This anisotropy is expected to originate from the particle surface. So, the results are interpreted by a simple model, in which each single-domain nanoparticle is considered as a core–shell system with magnetocrystalline anisotropy on the core and surface anisotropy on the shell.

5.2 Sample: $Co_{0.3}Zn_{0.7}Fe_2O_4$

In this section, the magnetic properties of $Co_{0.3}Zn_{0.7}Fe_2O_4$ nanoparticles synthesized by PEG assisted hydrothermal method were investigated by superparamagnetic resonance (SPR) technique by using conventional X-band (f @ 9.5 GHz) Bruker EMX model spectrometer. The first derivative of microwave power absorbed by the sample with respect to the static magnetic field, *dP/dH,* is plotted as a function of static field for some selected temperatures as shown in Figure 5.6.

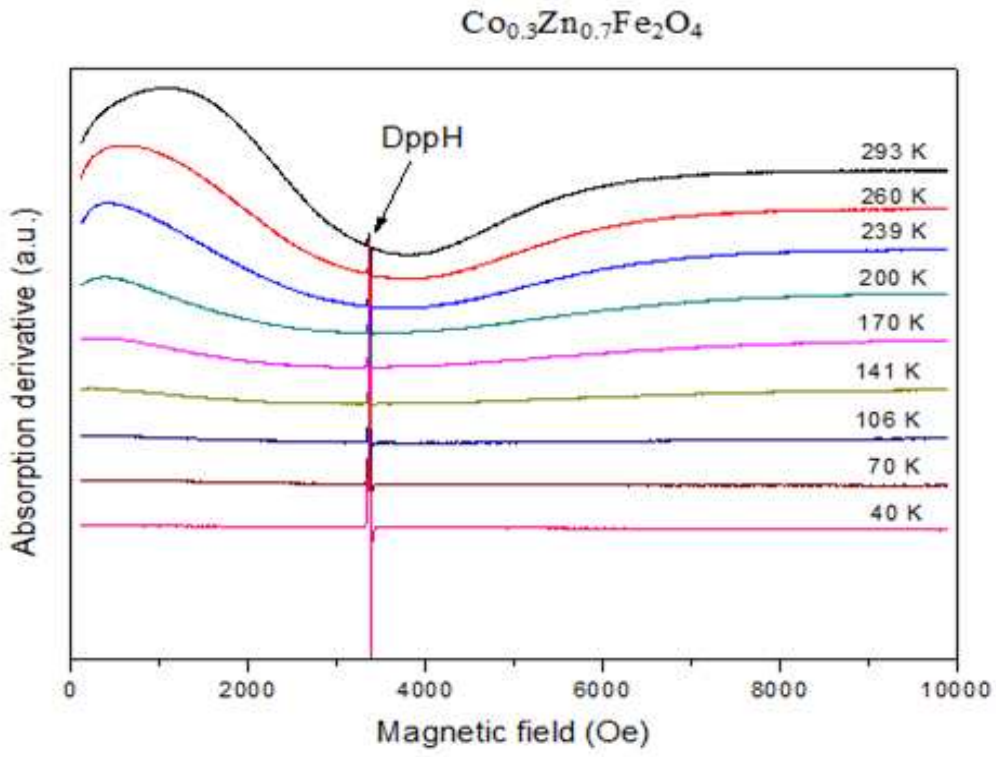

Figure 5.6 SPR spectra of $Co_{0.3}Zn_{0.7}Fe_2O_4$ nanoparticles at some selected temperatures.

As it is seen from this figure, the resonance field and the line width of the SPR spectra are strictly temperature dependent. At room temperature, a single, strong and broad SPR signal was observed with the resonance field and the line width of 2402 G and 2716 G, respectively. It can be seen that the SPR signals taken from the sample are almost symmetric with respect to the resonance field Hr at all temperatures. Such a symmetric signal may be attributed to a single type of species. It should be noted that the signal amplitudes are given in arbitrary unit. As the temperature is decreased, the line broadens and shifts down to lower fields.

5.2.1 The linewidth

Figure 5.7 shows the temperature variation of the line width values of the SPR spectra of $Co_{0.3}Zn_{0.7}Fe_2O_4$ nanoparticles. As seen from the figure, the line width increases as the temperature decreases down to 240 K and decreases smoothly between 240-170 K. Then, below 170 K, a sharp increase in the line width is observed down to 120 K. Below this temperature, the intensity of the SPR signal goes to zero, therefore it is not possible to measure the line width. It is known that, in a randomly oriented ferromagnet the absorption line width follows a non-monotonic function of temperature. At low temperatures the line width is large due to the scattering in direction of anisotropic field of particles (inhomogeneous broadening). As the temperature increases the tendency to make magnetic moment isotropic causes the line width to decrease.

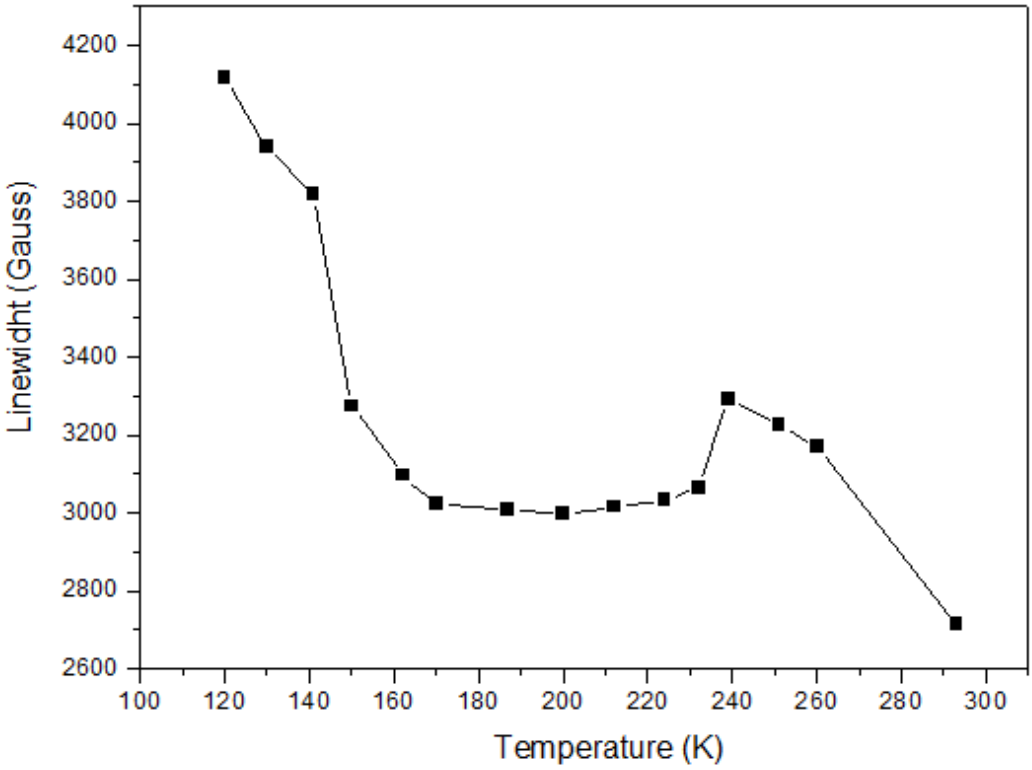

Figure 5.7 Temperature variation of SPR linewidth.

5.2.2 The resonance field

Figure 5.8 shows the variation of the resonance field values (measured from the magnetic field at the center of the SPR resonance curve or the field where the maximum absorption takes place) with the temperature. The figure implies that the resonance field decreases when the temperature decreases down to 140 K. Below this temperature the resonance field increases sharply down to 40 K. And no measurement can be done below 40 K, since the signal intensity goes to almost zero and the SPR signal line width expands too much.

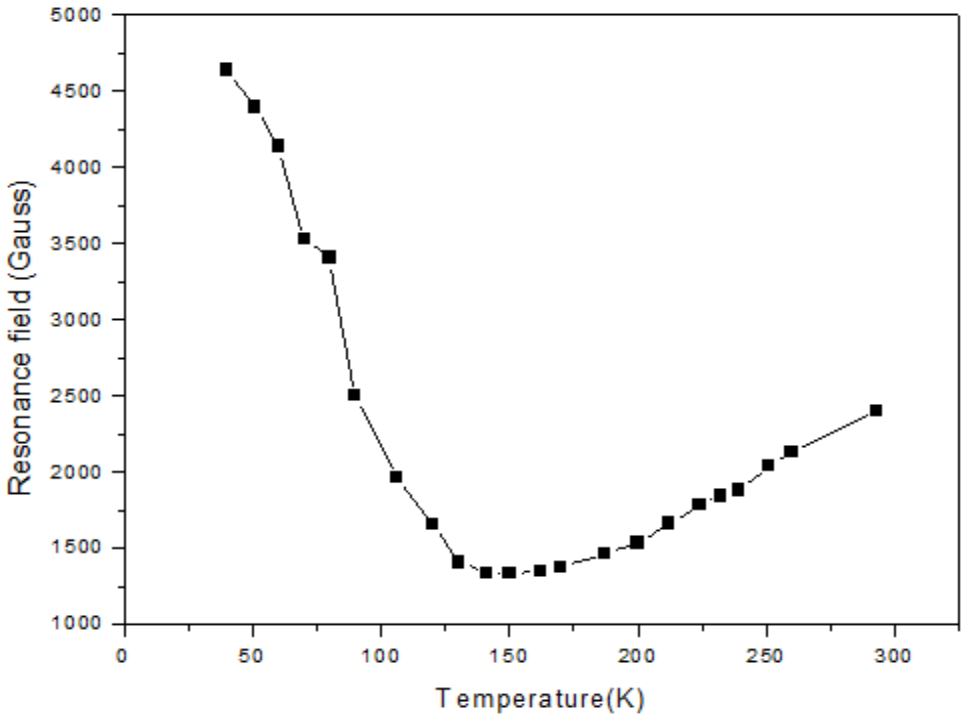

Figure 5.8 Temperature dependence of apparent SPR resonance field and the theoretical fit.

5.2.3 Anisotropy field

Figure 5.9 indicates the temperature variation of the anisotropy field (obtained by B(290 K) – B(T)) for the sample $Co_{0.3}Zn_{0.7}Fe_2O_4$. As it can be seen from the figure that, the anisotropy field of the sample is increasing sharply by the temperature between 140 K and the lowest temperature, above this temperature it is slightly decreasing by the temperature. It reaches a maximum anisotropy field of 1062 G at around 140 K.

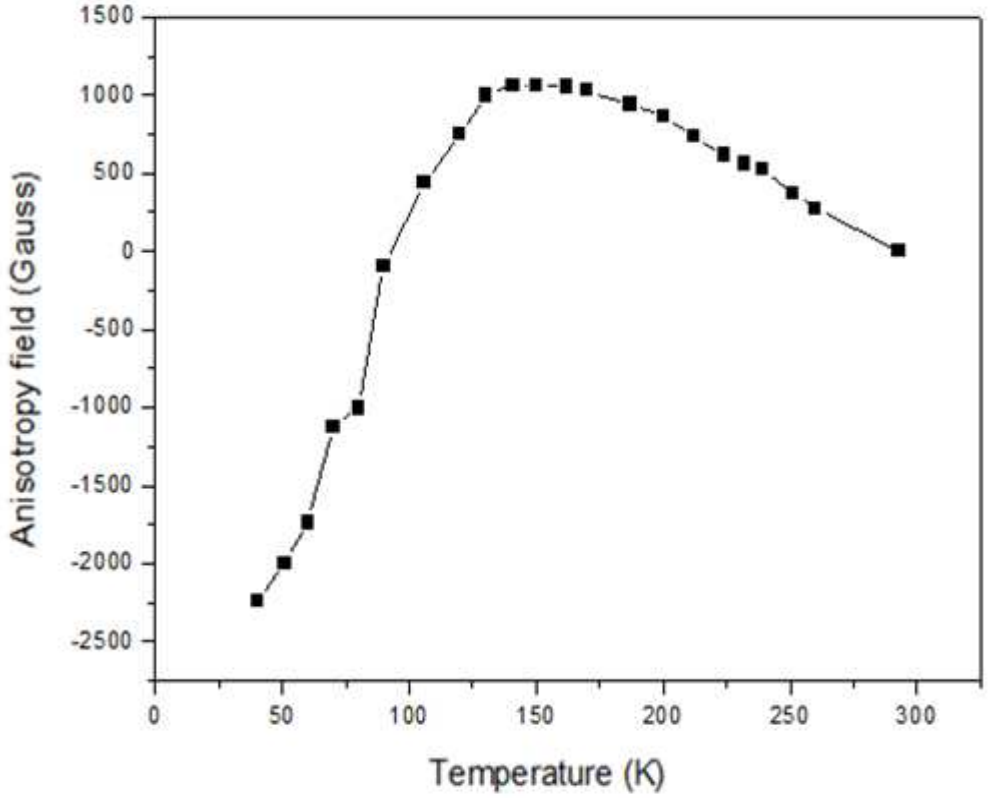

Figure 5.9 Anisotropy field values obtained by B(290 K) – B(T).

Between the room temperature and 140 K, by decreasing the temperature, as the shell spins increase their magnetic susceptibility, they produce an effective field on the core,leading to a decrease of the resonance field from its high temperature value. As the shell spins begin to order the effective anisotropy increases, following its surface value more closely.

5.2.4 The SPR intensity

Figure 5.10 shows the temperature dependence of the SPR spectra intensity obtained by double integration of the experimental derivative of absorption spectra. One can see that this dependence is quite similar to that observed for the zero field cooled (ZFC) magnetic susceptibility of $Co_{0.3}Zn_{0.7}Fe_2O_4$ nanoparticles [20, 53, 91,92].

Figure 5.10 implies that the intensity sharply decreases when the temperature decreases down to 180 K. Below this temperature the intensity increases slightly between 180-130 K. Between 130 K and 70 K, it increases slightly by decreasing the temperature. Below 70 K, it decreases smoothly down to 40. And, no SPR measurements could be done

below 40 K, since the signal intensity goes almost to zero and the SPR signal is shifted to higher fields.

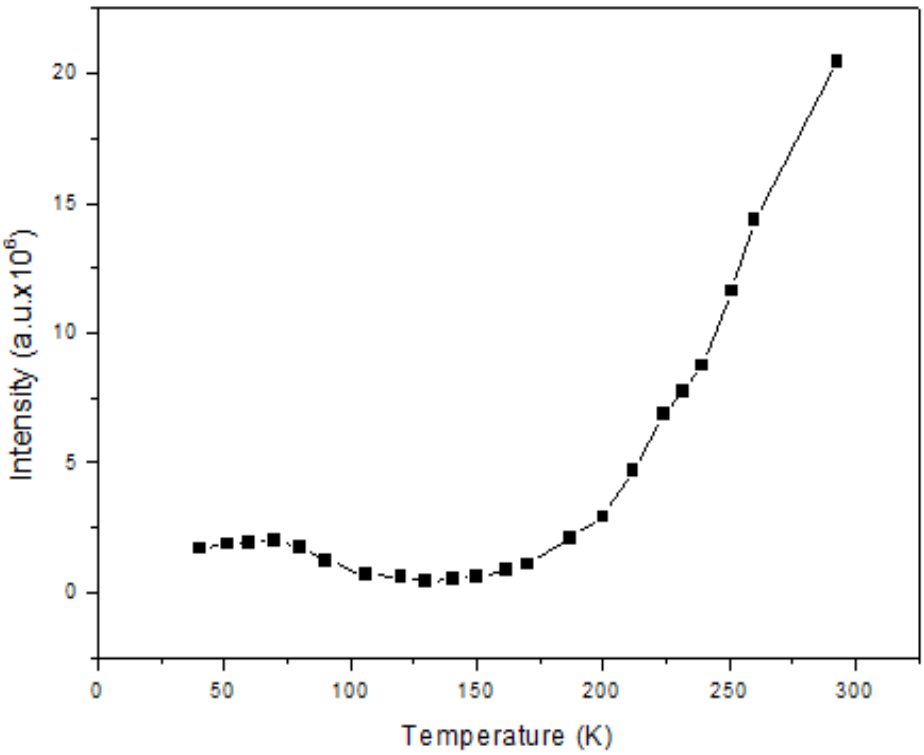

Figure 5.10 SPR intensity values obtained by double integration of signals.

5.2.5 Summary for $Co_{0.3}Zn_{0.7}Fe_2O$ nanoparticles

The SPR spectra of the $Co_{0.3}Zn_{0.7}Fe_2O_4$ nanoparticles show a single, relatively broad signal. The SPR spectra at low temperatures become very broad (with the peak to peak line width comparable to the apparent resonance field at the X-band) and the resonance field shift towards lower magnetic fields. We remark the existence magnetic phase change between high and low temperature region. In the high-temperature regime we observed a ferromagnetic behaviour with high anisotropy. Since the size of the sample is too small, the anisotropy is caused by the core anisotropy at high temperatures. At low temperature regime, the experiments show signs of a decreasing anisotropy by the decrease of temperature. At the lowest temperature a smallest anisotropy was observed. This anisotropy is expected to

originate from the particle surface. So, the results are interpreted by a simple model, in which each single-domain nanoparticle is considered as a core–shell system, with magneto-crystalline anisotropy on the core and surface anisotropy on the shell. Below 140 K, antiferromagnetic effects become dominant. These can be attributed to the high anisotropic behavior of cobalt ions.

CHAPTER 6

CONCLUSIONS

Magnetic properties of $ZnFe_2O_4$ and $Co_{0.3}Zn_{0.7}Fe_2O_4$ nanoparticles have been studied by superparamagnetic resonance (SPR) in terms of temperature. Strong temperature dependence of SPR spectra of the samples was observed. While the resonance field is decreasing by decreasing temperature, the peak to peak line width is increasing. At low temperatures, the anisotropy energy KV is larger than the thermal energy k_BT to render the nanoparticles to be blocked readily. At even lower temperatures, the anisotropy energy of magnetic nanoparticles enhanced too much. The enhancement of the line width and the anisotropy is increased at low temperatures. Since the relation between the blocking temperature and the particle volume is given as follows [52, 93]:

$$T_B = KV / k_B \ln ft \qquad (6.1)$$

When the volume of the nanoparticles decreased, the blocking temperature is also decreased as seen from the line width, resonance field, and the anisotropy field graphs. Where t is the experimental measuring time, K is the anisotropy energy density constant and V is the volume of the particle. The particles with very small size distribution showed the blocking temperatures below the room temperature.

From SPR measurements it was observed that $ZnFe_2O_4$ nanoparticles indicate paramagnetic behavior at high temperatures, superparamagnetic behavior at around the blocking temperature and ferromagnetic behavior below the blocking temperature. Where as, $Co_{0.3}Zn_{0.7}Fe_2O_4$ nanoparticles show ferromagnetic behavior at high temperatures and indicate

antiferromagnetic behavior below 140 K. As a result, the magnetic behaviors are changing too much with the inclusion of cobalt ions. This can be attributed to high cobalt anisotropy.

REFERENCES

[1] http://physics.about.com/od/physics101thebasics/f/fund_forces.htm.

[2] Z. H. Zhou, J. Wang, J. M. Xue and H. S. O. Chan, J. Mater. Chem,11 (2001) 3110.

[3] V. Raul, Magnetic Ceramics, Cambridge University Press, Cambridge, UK, (1994).

[4] L. L. Beecroft and C. K. Ober, Chem. Mater. 9 (1997) 1302.

[5] A. Yasumori, H. Matsumoto, S. Hayashi and K. Okada, J Sol–Gel Sci. Technol., 18 (2000) 249.

[6] R. F. Ziolo, E. P. Giannelis, B. A. Weinstein, M. P. O'Horo,B. N. Ganguly, V. Mehrotra, M. W. Russell and D. R. Huffman,Science, 257 (1992) 219.

[7] B. H. Sohn, R. E. Cohen and G. C. Papaefthymiou, J. Magn.Magn. Mater., 182(1998) 216.

[8] C. Castro, J. Ramos, A. Millan, J. G. Calbet and F. Palacio, Chem.Mater.,12 (2000) 3681.

[9] F. D. Monte, M. P. Morales, D. Levy, A. Fernandez, M. Ocana,A. Roig, E. Molins, K. O'Grady and C. J. Serna, Langmuir, 13 (1997) 3627.

[10] F. Bentivegna, J. Ferre, M. Nyvlt, J. P. Jamet, D. Imhoff,M. Canva, A. Brun, P. Veillet, S. Visnovsky, F. Chaput andJ. P. Boilot, J. Appl. Phys., 83 (1998) 7776.

[11] http://lib.bioinfo.pl/blid:1739.

[12] C. Yao, Q. Zeng, G.F.Goya, T.Torres, J. Liu, H. Wu, M. Ge, Y. Zeng, Y. Wang, and J.Z.Jiang, J.Phys.Chem.C ,111 (2007) 12274.

[13] C. R .Alves, R. Aquino, J. Depeyrot, T. A. P Cotta, M. H .Sousa, F. A. Tourinho, H. R.Rechenberg , G. F .Goya. J. Appl. Phys., 99 (2006) 08M905.

[14] Y. Köseoğlu, A. Baykal, M. S. Toprak, F. Gözüak, A. C. Başaran, B. Aktaş, Journal of Alloys and Compounds 462 (2008) 209.

[15] R.H. Kodama, J.Magn. Magn. Mater. 200 (1999) 359.

[16] R.D.K. Misra, A. Kale, R.S. Srivatsava, O. Senkov, Mater. Sci. Technol.19 (2003) 826.

[17] R.D.K. Misra, A. Kale, B. Hooi, J.Th. DeHosson, Mater. Sci. Technol.,19 (2003) 1617.

[18] Z.H. Zhou, J.M. Xue, J. Wang, H.S.O. Chan, T. Yu, Z.X. Shen, J. Appl. Phys. 91 (2002) 6015.

[19] Y.Köseoğlu F. Yıldız, B. Aktas¸, G.S. Alvarez, M. Toprak, M. Muhammed,

Phys. Stat. Sol. B 242 (2005) 1712.

[20] Y. Köseoğlu, H. Kavas, and B. Aktaş, phys. stat. sol. (a) 203, No.7 (2006) 1595.

[21] J. Popplewell, L. Sakhnini, J. Magn. Magn. Mater. 149 (1995) 72.

[22] K. Raj, B. Moskowitz, R. Casciari, J. Magn. Magn. Mater. 149 (1995) 174.

[23] D.K. Kim, Y. Zhang, J. Kehr, T. Klason, B. Bjelke, M. Muhammed, J.Magn. Magn. Mater. 225 (2001) 256.

[24] Y.Köseoğlu , B. Aktas, Phys. Stat. Sol. C 1 (2004) 3516.

[25] D.K. Kim, Y. Zhang, W. Voit, K.V. Rao, J. Kehr, T. Klason, B. Bjelke, M. Muhammed, Scripta Mater. 44 (2001) 1713.

[26] E.J.W. Verwey, Nature 144 (1939) 327.

[27] B. Aktas, Thin Sold Films 307 (1997) 250.

[28] R.W. Chantrell, G.N. Coverdale, M. El Hilo, K. O'Grady, J. Magn. Magn.Mater. 157/158 (1996) 250.

[29] V.I. Nikolaev, T.A. Bushina, K.E. Chan, J. Magn. Magn. Mater. 213 (2000) 213.

[30] J.T. Lue, J. Phys. Chem. Solids 62 (2001) 1599.

[31] M.F. Hansen, S. Morup, J. Magn. Magn. Mater. 184 (1998) 262.

[32] www.ele.auckland.ac.nz/~kacprzak/notes.htm.

[33] http://www.irm.umn.edu/hg2m/hg2m.pdf.

[34] http://www.doitpoms.ac.uk/tlplib/ferromagnetic/types.php.

[35] http://en.wikipedia.org/wiki/Ferromagnetism.

[36] www.electronics-tutorials.ws/electromagnetism.

[37] R.A. Serway, R.J. Beicher, R. McGrew, J. Soul, C. Teague, Physics for Scientists and Engineers, 5th Ed., Sunders College Pub., (2003).

[38] http://hyperphysics.phy-astr.gsu.edu/hbase/HFrame.html.

[39] H. Kavas, Superparamagnetic resonance studies on magnetic nanoparticles, Master Thesis, Fatih University, (2006).

[40] B.D. Cullity, Introduction to Magnetic Materials, Addison-Wesley Publishing Company, Philippines, (1972).

[41] http://en.wikipedia.org/wiki/Superparamagnetism.

[42] http://lmis1.epfl.ch/webdav/site/lmis1/shared/Files/Lectures/Nanotechnology%20 for %20 engineers/Archives/2004_05/Superparamagnetism.pdf.

[43] C. M. Sorensen, in Nanoscale Materials in Chemistry (Ed.: K. J.Klabunde), John Wiley and Sons, Inc., New York, (2001), pp. 169.114.

[44] C. Kittel, Introduction to Solid State Physics, Wiley, New York, (1976).

[45] R. H. Kodama, A. E. Berkowitz, Physical Review B , 59 (1999) 6321.

[46] M. Ozaki, in Fine Particles: Synthesis, Characterization, and Mechanisms of Growth, Vol. 92 (Ed.: T. Sugimoto), Marcel Dekker, Inc., New York,(2000).

[47] I. S. Jacobs, C. P. Bean, in Magnetism, Vol. III (Eds.: G. T. Rado, H.Suhl), Academic Press, New York, (1963), pp. 271.

[48] http:// nanospinel.blokspot.com/2007/ 11/magnetic-studies-on -zinc ferrites. html.

[49] E. C. Stoner and E. P. Wohlfarth, Philos. Trans. London Ser., 1948, A 240,599.

[50] L. Neel, Ann. Geophys., 5 (1949) 99.

[51] W. F. Brown, Jr., Phys. Rev., 130 (1963) 1677.

[52] Y. Köseoğlu and H. Kavas J. Nanosci. Nanotechnol., Vol. 8, No. 2 (2008) 1533- 4880/2008/8/584/007, Doi:10.1166/jnn.2008.B012.

[53] R. Berger, J. Bissey, J. Kliava, H. Daubric, and C. Estournes, J. Magn. Magn. Mater., 234 (2001) 535.

[54] R. Berger, J. C. Bissey, and J. Kliava, J. Phys.: Condens. Matter ., 12 (2000) 9347

[55] E. De Biasi, C. A. Ramos, R.D.Zysler , andH.Romero, Physica B, 354 (2004) 286.

[56] C.N. Chinnasamy, A. Narayanasamy, N. Ponpandian, K. Chattopadhyay, H. Gue´rault, J-M. Greneche, Scripta Mater. 44 (2001) 1407.

[57] T. Sato, K. Haneda, M. Seki, and T. Iijima, Appl. Phys. A., 50 (1990) 13.

[58] B. Jeyadevan, K. Tohji, K. Nakatsuka, and A. Narayanasamy, J. Magn. Magn. Mater . 99 (2000) 217.

[59] S. A. Oliver, H. H. Hamdeh, and J. C. Ho, Phys. Rev. B. 60 (1999) 3400.

[60] F. J. Burghart, et al., Phys. B., 286 (2000) 289.

[61] J. Z. Jiang, P. Wynn, S. Mørup, T. Okada, and F. J. Berry, Nanostruct. Mater. 12 (1999) 737.

[62] G. F. Goya and H. R. Rechenberg, J. Magn. Magn. Mater. 196(1999) 191.

[63] X.F. Chu, X.Q. Liu, G.Y. Meng, Sens. Actuators B 55 (1999) 19.

[64] S.V.Manorama, L. Satyaranaya, K.M. Reddy, Sens. Actuators B 89 (2003)62.

[65] L. Neel, Comput. Rend. 252 (1961) 4075.

[66] H. Nathani, R.D.K. Misra, Mater. Sci. Eng. B 113 (2004) 228.

[67] N. Kasapoglu, B. Birsöz, A. Baykal, Y. Köseoğlu, M.S. Toprak, Central Eur. J.Chem. 5 (2) (2007) 570.

[68] http://wikis.lib.ncsu.edu/index.php/Spinel.

[69] A.M. R. De. F. Teixeira, T. Ogasawara**,** M. C. De. S. Nóbrega Materials Research, Vol. 9, No. 3 (2006) 257.

[70] R.Arulmurugan ,B. Jeyadevan , G.Vaidyanathan , Sendhilnathan S. J .Magn Magn Mater. , 288 (2005) 470.

[71] Virden AE, O'Grady K. J Magn Magn Mater. 868 (2005) 290.

[72] S.Verma , P.A. Joy , Y.B. Khollam , H.S. Potdar, S.B. Deshpande. Mater Lett., 58(6) (2004) 1092.

[73] F. Gözüak, Synthesis and magnetic characterization of $Co_xZn_{1-x}Fe_2O_4$ nanoparticles, Master Thesis, Fatih University, (2008).

[74] D. S. Mathew, R. S. Juang. Chemical Engineering Journal, 129 (2007) 1.

[75] A.C.F. Costa, E.Tortella, E.F. Neto, Morelli MR, R.H.G.A. Kiminami. Mater Res. 7(4) (2004) 523.

[76] D.S. Ghose J. Mater Res Bull. ,38(11-12) (2003) 1653.

[77] P.B. Pandya, H.H. Joshi, R.G. Kulkarni. J Mater Sci., 26(20) (1991) 5509.

[78] K. Suzuki, Jpn J Appl Phys., 27(3) (1988) 361.

[79] M.A.Ahmed Phys Stat Sol A. ,111 (1989) 56772.

[80] A. Tawfik. J Therm Anal.,35 (1989) 141.

[81] S.R Murthy, R. Seshagiri .J Less Common Met., 65 (1979) 19.

[82] S.R.Murthy. J Mater Sci Lett. 1984; 3:1049-51.

[83] M.I. Abd El-Ati, M.A .Kafafy, A. Acta Phys Pol A., 79(6) (1991) 889.

[84] G.A.Gaballa ,Phase Transitions, 46 (1994) 66.

[85] N.Z. Darwish, O.M.Hemeda, M.I. Abd El-Ati. Appl Radiat Isot. 45(4):445.

[86] E. De Biasi, R. D. Zysler, C. A. Ramos, and H. Romero, J. Magn. Magn. Mater., 87 (2005) 294.

[87] Misbah-ul-Islam, K. A. Hashmi, M.U. Rana, T. Abbas, Solid State Communications 121 (2002) 51.

[88] R.H. Kodama, A.E. Berkowitz, E.J. McNiff, Jr.S. Foner, J. Appl. Phys. 81 (1997) 5552.

[89] Landolt-Börnstein, New Series III/4b, Springer, New York, (1970).

[90] R.D.Zysler , H.Romero, C.A.Ramos, E.De Biasi, and D.Fiorani, J. Magn. Magn. Mater., 266 (2003) 233.

[91] P. Brahma, S. Banerjee, D. Das, P. K. Mukhopadhyay, S. Chatterjee, A. K. Nigam, and D. Chakravorty, J. Magn. Magn. Mater., 246 (2002) 162.

[92] L. Horng, G. Chern, M. C. Chen, P. C. Kang, and D. S. Lee, J. Magn. Magn. Mater. 389 (2004) 270.

[93] J.Chatterjee, Y.Haik, and C.J.Chen, J. Magn. Magn. Mater., 257 (2003) 113.